

**Enclosure 2**

**MFN 10-276**

**NEDO-33326-A, Revision 1, "GE14E for ESBWR Initial  
Core Nuclear Design Report"**

**Non-Proprietary Information**



**Global Nuclear Fuel**

**A Joint Venture of GE, Toshiba, & Hitachi**

**NEDO-33326-A**

**Revision 1**

**Class I**

**eDRF-0000-0067-3427**

**September 2010**

**Licensing Topical Report**

**GE14E FOR ESBWR INITIAL CORE  
NUCLEAR DESIGN REPORT**

*COPYRIGHT 2007-2010 GLOBAL NUCLEAR FUELS-AMERICAS, LLC  
ALL RIGHTS RESERVED*

### **INFORMATION NOTICE**

This document is the non-proprietary version of NEDC-33326P-A, Revision. 1, and thus, has the proprietary information removed. Portions of this document that have been removed are indicated by open and closed double brackets, as shown here [[ ]].

### **IMPORTANT NOTICE REGARDING CONTENTS OF THIS REPORT**

#### **Please Read Carefully**

The information contained in this document is furnished as reference material for GE14E for ESBWR, Initial Core Nuclear Design Report. The only undertakings of Global Nuclear Fuel (GNF) with respect to information in this document are contained in the contracts between GNF and the participating utilities in effect at the time this report is issued, and nothing contained in this document shall be construed as changing those contracts. The use of this information by anyone other than that for which it is intended is not authorized; and with respect to any unauthorized use, GNF makes no representation or warranty, and assumes no liability as to the completeness, accuracy, or usefulness of the information contained in this document.

Copyright, Global Nuclear Fuel (GNF), 2007-2010

## **CHANGES FROM NEDO-33326 REVISION 1 TO NEDO-33326-A REVISION 1**

### **Purpose**

The purpose of NEDO-33326-A Revision 1 is to document the NRC's acceptance of this Licensing Topical Report.

### **Summary of Revisions**

NEDO-33326-A Revision 1 incorporates the NRC letter indicating their acceptance of this revision of this Licensing Topical Report as well as Enclosure 1 of the letter, which contains the Final Safety Evaluation for this Licensing Topical Report. These items have been added at the end of the report as Attachment 1.

## **CHANGES FROM REVISION 0 TO REVISION 1**

### **Purpose**

The purpose of Revision 1 is to document a reconfigured initial core design that was optimized at a lower TRACG predicted core flow. The lower predicted core flow can be attributed to a correction of the GE14E spacer loss coefficients in the TRACG simulations. The spacer loss coefficients have now been consistently applied in TRACG and in PANACEA based on the same measured pressure drop data base. Standard BWR core design options were exercised in order to improve thermal margins at the lower core flow. These options included:

- Bundle shuffling to flatten radial power. This was primarily accomplished by the removal of sixteen low reactivity control cells in the peripheral core region.
- Control rod pattern changes, with major sequence adjustments performed every 2500 MWd/ST.
- Simplification of core loading inventory, i.e., the number of bundle types was reduced from six to five.

The reconfigured initial core design with key performance results are documented in this revision.

### **Summary of Revisions**

1. Section 2 provides detailed design information for the five remaining bundles used in the initial core. Design data for the sixth bundle is no longer shown.
2. Section 3 should be considered entirely new since the majority of the section was updated with new core design information and evaluation results. In addition, the reactivity coefficients have been calculated with xenon, which represents a more conservative analysis condition.

## TABLE OF CONTENTS

<b>1.</b>	<b>NUCLEAR DESIGN BASIS.....</b>	<b>1-1</b>
1.1	NEGATIVE REACTIVITY FEEDBACK BASES.....	1-1
1.2	CONTROL REQUIREMENTS (SHUTDOWN MARGINS) .....	1-1
1.3	CONTROL REQUIREMENTS (OVERPOWER BASES) .....	1-1
1.3.1	<i>Maximum Linear Heat Generation Rate.....</i>	<i>1-2</i>
1.3.2	<i>Minimum Critical Power Ratio.....</i>	<i>1-2</i>
1.4	CONTROL REQUIREMENTS (STANDBY LIQUID CONTROL SYSTEM) .....	1-2
1.5	STABILITY BASES.....	1-2
<b>2.</b>	<b>BUNDLE DESIGN EVALUATION.....</b>	<b>2-1</b>
2.1	INTRODUCTION .....	2-1
2.2	BUNDLE AND LATTICE DESIGNS .....	2-1
2.2.1	<i>GE14E Bundle Design Features for Initial Core.....</i>	<i>2-2</i>
2.2.2	<i>Bundle Local Peaking.....</i>	<i>2-2</i>
2.2.3	<i>Bundle R-Factor.....</i>	<i>2-2</i>
2.2.4	<i>Doppler Reactivity Coefficient.....</i>	<i>2-2</i>
2.3	SUMMARY .....	2-3
<b>3.</b>	<b>CORE NUCLEAR DESIGN EVALUATION.....</b>	<b>3-1</b>
3.1	NUCLEAR DESIGN AND CORE LOADING PATTERN DESCRIPTION .....	3-1
3.2	EIGENVALUE DETERMINATION .....	3-2
3.3	CONTROL ROD PATTERNS INCLUDING AXIAL POWER CONSIDERATIONS.....	3-2
3.4	INTEGRATED POWER DISTRIBUTION .....	3-3
3.5	THERMAL LIMIT EVALUATION.....	3-3
3.5.1	<i>MLHGR.....</i>	<i>3-3</i>
3.5.2	<i>MCPR.....</i>	<i>3-4</i>
3.6	HOT EXCESS EVALUATION.....	3-4
3.7	COLD SHUTDOWN MARGIN EVALUATION.....	3-5
3.8	STANDBY LIQUID CONTROL SYSTEM EVALUATION .....	3-6
3.9	CRITICALITY OF REACTOR DURING REFUELING EVALUATION.....	3-6
3.10	NEGATIVE REACTIVITY FEEDBACK EVALUATION.....	3-6
3.10.1	<i>Moderator Temperature Coefficient Evaluation.....</i>	<i>3-6</i>
3.10.2	<i>Moderator Void Coefficient Evaluation.....</i>	<i>3-7</i>
3.11	XENON STABILITY EVALUATION .....	3-7
3.11.1	<i>BWR Xenon Trends.....</i>	<i>3-8</i>
3.11.2	<i>ESBWR Xenon Transient Conclusions.....</i>	<i>3-9</i>
3.12	SUMMARY .....	3-9
<b>4.</b>	<b>REFERENCES.....</b>	<b>4-1</b>

## LIST OF FIGURES

FIGURE 2-1. BUNDLE DESIGN FOR 2990 .....	2-4
FIGURE 2-2. FUEL RODS FOR 2990.....	2-5
FIGURE 2-3. FUEL RODS FOR 2990 .....	2-6
FIGURE 2-4. SPLITS AND WEIGHTS FOR 2990.....	2-7
FIGURE 2-5. BUNDLE DESIGN FOR 2991 .....	2-8
FIGURE 2-6. FUEL RODS FOR 2991.....	2-9
FIGURE 2-7. FUEL RODS FOR 2991.....	2-10
FIGURE 2-8. SPLITS AND WEIGHTS FOR 2991.....	2-11
FIGURE 2-9. BUNDLE DESIGN FOR 2992 .....	2-12
FIGURE 2-10. FUEL RODS FOR 2992 .....	2-13
FIGURE 2-11. FUEL RODS FOR 2992 .....	2-14
FIGURE 2-12. SPLITS AND WEIGHTS FOR 2992.....	2-15
FIGURE 2-13. BUNDLE DESIGN FOR 2993 .....	2-16
FIGURE 2-14. FUEL RODS FOR 2993 .....	2-17
FIGURE 2-15. FUEL RODS FOR 2993 .....	2-18
FIGURE 2-16. SPLITS AND WEIGHTS FOR 2993.....	2-19
FIGURE 2-17. BUNDLE DESIGN FOR 2994 .....	2-20
FIGURE 2-18. FUEL RODS FOR 2994 .....	2-21
FIGURE 2-19. FUEL RODS FOR 2994 .....	2-22
FIGURE 2-20. SPLITS AND WEIGHTS FOR 2994.....	2-23
FIGURE 2-21. LATTICE 7632 K-INFINITY .....	2-24
FIGURE 2-22. LATTICE 7633 K-INFINITY .....	2-25
FIGURE 2-23. LATTICE 7634 K-INFINITY .....	2-26
FIGURE 2-24. LATTICE 7635 K-INFINITY .....	2-27
FIGURE 2-25. LATTICE 7636 K-INFINITY .....	2-28
FIGURE 2-26. LATTICE 7637 K-INFINITY .....	2-29
FIGURE 2-27. LATTICE 7638 K-INFINITY .....	2-30
FIGURE 2-28. LATTICE 7639 K-INFINITY .....	2-31
FIGURE 2-29. LATTICE 7640 K-INFINITY .....	2-32
FIGURE 2-30. LATTICE 7641 K-INFINITY .....	2-33
FIGURE 2-31. LATTICE 7642 K-INFINITY .....	2-34
FIGURE 2-32. LATTICE 7643 K-INFINITY .....	2-35
FIGURE 2-33. LATTICE 7644 K-INFINITY .....	2-36
FIGURE 2-34. LATTICE 7645 K-INFINITY .....	2-37
FIGURE 2-35. LATTICE 7646 K-INFINITY .....	2-38
FIGURE 2-36. LATTICE 7647 K-INFINITY .....	2-39
FIGURE 2-37. LATTICE 7648 K-INFINITY .....	2-40
FIGURE 2-38. LATTICE 7649 K-INFINITY .....	2-41
FIGURE 2-39. LATTICE 7650 K-INFINITY .....	2-42
FIGURE 2-40. LATTICE 7651 K-INFINITY .....	2-43
FIGURE 2-41. LATTICE 7652 K-INFINITY .....	2-44
FIGURE 2-42. LATTICE 7653 K-INFINITY .....	2-45
FIGURE 2-43. LATTICE 7654 K-INFINITY .....	2-46
FIGURE 2-44. LATTICE 7655 K-INFINITY .....	2-47
FIGURE 2-45. LATTICE 7632 MAXIMUM LOCAL PEAKING .....	2-48
FIGURE 2-46. LATTICE 7633 MAXIMUM LOCAL PEAKING .....	2-49
FIGURE 2-47. LATTICE 7634 MAXIMUM LOCAL PEAKING .....	2-50

## LIST OF FIGURES

FIGURE 2-48. LATTICE 7635 MAXIMUM LOCAL PEAKING .....	2-51
FIGURE 2-49. LATTICE 7636 MAXIMUM LOCAL PEAKING .....	2-52
FIGURE 2-50. LATTICE 7637 MAXIMUM LOCAL PEAKING .....	2-53
FIGURE 2-51. LATTICE 7638 MAXIMUM LOCAL PEAKING .....	2-54
FIGURE 2-52. LATTICE 7639 MAXIMUM LOCAL PEAKING .....	2-55
FIGURE 2-53. LATTICE 7640 MAXIMUM LOCAL PEAKING .....	2-56
FIGURE 2-54. LATTICE 7641 MAXIMUM LOCAL PEAKING .....	2-57
FIGURE 2-55. LATTICE 7642 MAXIMUM LOCAL PEAKING .....	2-58
FIGURE 2-56. LATTICE 7643 MAXIMUM LOCAL PEAKING .....	2-59
FIGURE 2-57. LATTICE 7644 MAXIMUM LOCAL PEAKING .....	2-60
FIGURE 2-58. LATTICE 7645 MAXIMUM LOCAL PEAKING .....	2-61
FIGURE 2-59. LATTICE 7646 MAXIMUM LOCAL PEAKING .....	2-62
FIGURE 2-60. LATTICE 7647 MAXIMUM LOCAL PEAKING .....	2-63
FIGURE 2-61. LATTICE 7648 MAXIMUM LOCAL PEAKING .....	2-64
FIGURE 2-62. LATTICE 7649 MAXIMUM LOCAL PEAKING .....	2-65
FIGURE 2-63. LATTICE 7650 MAXIMUM LOCAL PEAKING .....	2-66
FIGURE 2-64. LATTICE 7651 MAXIMUM LOCAL PEAKING .....	2-67
FIGURE 2-65. LATTICE 7652 MAXIMUM LOCAL PEAKING .....	2-68
FIGURE 2-66. LATTICE 7653 MAXIMUM LOCAL PEAKING .....	2-69
FIGURE 2-67. LATTICE 7654 MAXIMUM LOCAL PEAKING .....	2-70
FIGURE 2-68. LATTICE 7655 MAXIMUM LOCAL PEAKING .....	2-71
FIGURE 2-69. ROD LOCAL PEAKING (BUNDLE 2990, LATTICE 7633, VF=40%, BOL).....	2-72
FIGURE 2-70. ROD LOCAL PEAKING (BUNDLE 2991, LATTICE 7638, VF=40%, BOL).....	2-73
FIGURE 2-71. ROD LOCAL PEAKING (BUNDLE 2992, LATTICE 7644, VF=40%, BOL).....	2-74
FIGURE 2-72. ROD LOCAL PEAKING (BUNDLE 2993, LATTICE 7648, VF=40%, BOL).....	2-75
FIGURE 2-73. ROD LOCAL PEAKING (BUNDLE 2994, LATTICE 7652, VF=40%, BOL).....	2-76
FIGURE 2-74. UNCONTROLLED ROD R-FACTORS (BUNDLE 2990, 20 GWD/ST).....	2-82
FIGURE 2-75. UNCONTROLLED ROD R-FACTORS (BUNDLE 2991, 20 GWD/ST).....	2-83
FIGURE 2-76. UNCONTROLLED ROD R-FACTORS (BUNDLE 2992, 20 GWD/ST).....	2-84
FIGURE 2-77. UNCONTROLLED ROD R-FACTORS (BUNDLE 2993, 20 GWD/ST).....	2-85
FIGURE 2-78. UNCONTROLLED ROD R-FACTORS (BUNDLE 2994, 20 GWD/ST).....	2-86
FIGURE 2-79. BUNDLE 2990 LATTICE 7633 K-INFINITY AT 40% VF .....	2-87
FIGURE 2-80. BUNDLE 2991 LATTICE 7638 K-INFINITY AT 40% VF .....	2-88
FIGURE 2-81. BUNDLE 2992 LATTICE 7644 K-INFINITY AT 40% VF .....	2-89
FIGURE 2-82. BUNDLE 2993 LATTICE 7648 K-INFINITY AT 40% VF .....	2-90
FIGURE 2-83. BUNDLE 2994 LATTICE 7652 K-INFINITY AT 40% VF .....	2-91
FIGURE 3-1. REFERENCE INITIAL CORE FUEL TYPES AND QUANTITIES .....	3-10
FIGURE 3-2. HOT DESIGN EIGENVALUE VS. EXPOSURE.....	3-11
FIGURE 3-3. COLD DESIGN EIGENVALUE VS. EXPOSURE .....	3-12
FIGURE 3-4. ROD PATTERNS.....	3-13
FIGURE 3-5. SEQUENCE 1 CORE AVERAGE AXIAL POWER DISTRIBUTIONS .....	3-21
FIGURE 3-6. SEQUENCE 2 CORE AVERAGE AXIAL POWER DISTRIBUTIONS .....	3-22
FIGURE 3-7. SEQUENCE 3 CORE AVERAGE AXIAL POWER DISTRIBUTIONS .....	3-23
FIGURE 3-8. SEQUENCE 4 CORE AVERAGE AXIAL POWER DISTRIBUTIONS .....	3-24
FIGURE 3-9. SEQUENCE 1 CORE AVERAGE AXIAL EXPOSURE DISTRIBUTIONS .....	3-25
FIGURE 3-10. SEQUENCE 2 CORE AVERAGE AXIAL EXPOSURE DISTRIBUTIONS .....	3-26
FIGURE 3-11. SEQUENCE 3 CORE AVERAGE AXIAL EXPOSURE DISTRIBUTIONS .....	3-27
FIGURE 3-12. SEQUENCE 4 CORE AVERAGE AXIAL EXPOSURE DISTRIBUTIONS .....	3-28

## LIST OF FIGURES

FIGURE 3-13. HOT EIGENVALUE VS. CYCLE EXPOSURE .....	3-29
FIGURE 3-14. END OF CYCLE BUNDLE AVERAGE EXPOSURE (10.98 GWD/ST) .....	3-30
FIGURE 3-15. RADIAL PEAKING FACTOR VS. CYCLE EXPOSURE.....	3-31
FIGURE 3-16. BEGINNING OF SEQUENCE 1 INTEGRATED BUNDLE POWER (0.0 GWD/ST).....	3-32
FIGURE 3-17. END OF SEQUENCE 1 INTEGRATED BUNDLE POWER (2.5 GWD/ST) .....	3-33
FIGURE 3-18. BEGINNING OF SEQUENCE 2 INTEGRATED BUNDLE POWER (2.5 GWD/ST).....	3-34
FIGURE 3-19. END OF SEQUENCE 2 INTEGRATED BUNDLE POWER (5.0 GWD/ST) .....	3-35
FIGURE 3-20. BEGINNING OF SEQUENCE 3 INTEGRATED BUNDLE POWER (5.0 GWD/ST).....	3-36
FIGURE 3-21. END OF SEQUENCE 3 INTEGRATED BUNDLE POWER (7.5 MWD/ST).....	3-37
FIGURE 3-22. BEGINNING OF SEQUENCE 4 INTEGRATED BUNDLE POWER (7.5 MWD/ST) .....	3-38
FIGURE 3-23. END OF SEQUENCE 4 INTEGRATED BUNDLE POWER (10.98 GWD/ST).....	3-39
FIGURE 3-24. MFLPD VS. CYCLE EXPOSURE .....	3-40
FIGURE 3-25. BEGINNING OF SEQUENCE 1 MFLPD (0.0 GWD/ST).....	3-41
FIGURE 3-26. END OF SEQUENCE 1 MFLPD (2.5 GWD/ST) .....	3-42
FIGURE 3-27. BEGINNING OF SEQUENCE 2 MFLPD (2.5 GWD/ST).....	3-43
FIGURE 3-28. END OF SEQUENCE 2 MFLPD (5.0 GWD/ST) .....	3-44
FIGURE 3-29. BEGINNING OF SEQUENCE 3 MFLPD (5.0 GWD/ST).....	3-45
FIGURE 3-30. END OF SEQUENCE 3 MFLPD (7.5 MWD/ST) .....	3-46
FIGURE 3-31. BEGINNING OF SEQUENCE 4 MFLPD (7.5 MWD/ST).....	3-47
FIGURE 3-32. END OF SEQUENCE 4 MFLPD (10.98 GWD/ST).....	3-48
FIGURE 3-33. MCPR VS. CYCLE EXPOSURE.....	3-49
FIGURE 3-34. BEGINNING OF SEQUENCE 1 MCPR (0.0 GWD/ST).....	3-50
FIGURE 3-35. END OF SEQUENCE 1 MCPR (2.5 GWD/ST).....	3-51
FIGURE 3-36. BEGINNING OF SEQUENCE 2 MCPR (2.5 GWD/ST).....	3-52
FIGURE 3-37. END OF SEQUENCE 2 MCPR (5.0 GWD/ST).....	3-53
FIGURE 3-38. BEGINNING OF SEQUENCE 3 MCPR (5.0 GWD/ST).....	3-54
FIGURE 3-39. END OF SEQUENCE 3 MCPR (7.5 MWD/ST).....	3-55
FIGURE 3-40. BEGINNING OF SEQUENCE 4 MCPR (7.5 GWD/ST).....	3-56
FIGURE 3-41. END OF SEQUENCE 4 MCPR (10.98 GWD/ST) .....	3-57
FIGURE 3-42. HOT EXCESS REACTIVITY VS. CYCLE EXPOSURE.....	3-58
FIGURE 3-43. HYDRAULIC CONTROL UNIT ASSIGNMENTS .....	3-59
FIGURE 3-44. COLD SHUTDOWN MARGIN VS. CYCLE EXPOSURE .....	3-60
FIGURE 3-45. CONTROL ROD WORTH COMPARISONS AT BOC (0.00 GWD/ST).....	3-61
FIGURE 3-46. CONTROL ROD WORTH COMPARISONS AT MOC (5.00 GWD/ST).....	3-62
FIGURE 3-47. CONTROL ROD WORTH COMPARISONS AT EOC (10.98 GWD/ST).....	3-63
FIGURE 3-48. COLD SHUTDOWN MARGIN DISTRIBUTION (%) AT BOC (0.0 GWD/ST) .....	3-64
FIGURE 3-49. COLD SHUTDOWN MARGIN DISTRIBUTION (%) AT MOC (5.0 GWD/ST) .....	3-65
FIGURE 3-50. COLD SHUTDOWN MARGIN DISTRIBUTION (%) AT EOC (10.98 GWD/ST) .....	3-66
FIGURE 3-51. STANDBY LIQUID CONTROL MARGIN VS. CYCLE EXPOSURE.....	3-67
FIGURE 3-52. EIGENVALUES VS. MODERATOR TEMPERATURE (FOR MTC) .....	3-68
FIGURE 3-53. MODERATOR TEMPERATURE COEFFICIENT .....	3-69
FIGURE 3-54. EIGENVALUES VS. MODERATOR TEMPERATURE (FOR MVC).....	3-70
FIGURE 3-55. MODERATOR VOID COEFFICIENT .....	3-71



## LIST OF TABLES

TABLE 2-1. LATTICE 7632 K-INFINITY .....	2-24
TABLE 2-2. LATTICE 7633 K-INFINITY .....	2-25
TABLE 2-3. LATTICE 7634 K-INFINITY .....	2-26
TABLE 2-4. LATTICE 7635 K-INFINITY .....	2-27
TABLE 2-5. LATTICE 7636 K-INFINITY .....	2-28
TABLE 2-6. LATTICE 7637 K-INFINITY .....	2-29
TABLE 2-7. LATTICE 7638 K-INFINITY .....	2-30
TABLE 2-8. LATTICE 7639 K-INFINITY .....	2-31
TABLE 2-9. LATTICE 7640 K-INFINITY .....	2-32
TABLE 2-10. LATTICE 7641 K-INFINITY .....	2-33
TABLE 2-11. LATTICE 7642 K-INFINITY .....	2-34
TABLE 2-12. LATTICE 7643 K-INFINITY .....	2-35
TABLE 2-13. LATTICE 7644 K-INFINITY .....	2-36
TABLE 2-14. LATTICE 7645 K-INFINITY .....	2-37
TABLE 2-15. LATTICE 7646 K-INFINITY .....	2-38
TABLE 2-16. LATTICE 7647 K-INFINITY .....	2-39
TABLE 2-17. LATTICE 7648 K-INFINITY .....	2-40
TABLE 2-18. LATTICE 7649 K-INFINITY .....	2-41
TABLE 2-19. LATTICE 7650 K-INFINITY .....	2-42
TABLE 2-20. LATTICE 7651 K-INFINITY .....	2-43
TABLE 2-21. LATTICE 7652 K-INFINITY .....	2-44
TABLE 2-22. LATTICE 7653 K-INFINITY .....	2-45
TABLE 2-23. LATTICE 7654 K-INFINITY .....	2-46
TABLE 2-24. LATTICE 7655 K-INFINITY .....	2-47
TABLE 2-25. LATTICE 7632 PEAKING .....	2-48
TABLE 2-26. LATTICE 7633 PEAKING .....	2-49
TABLE 2-27. LATTICE 7634 PEAKING .....	2-50
TABLE 2-28. LATTICE 7635 PEAKING .....	2-51
TABLE 2-29. LATTICE 7636 PEAKING .....	2-52
TABLE 2-30. LATTICE 7637 PEAKING .....	2-53
TABLE 2-31. LATTICE 7638 PEAKING .....	2-54
TABLE 2-32. LATTICE 7639 PEAKING .....	2-55
TABLE 2-33. LATTICE 7640 PEAKING .....	2-56
TABLE 2-34. LATTICE 7641 PEAKING .....	2-57
TABLE 2-35. LATTICE 7642 PEAKING .....	2-58
TABLE 2-36. LATTICE 7643 PEAKING .....	2-59
TABLE 2-37. LATTICE 7644 PEAKING .....	2-60
TABLE 2-38. LATTICE 7645 PEAKING .....	2-61
TABLE 2-39. LATTICE 7646 PEAKING .....	2-62
TABLE 2-40. LATTICE 7647 PEAKING .....	2-63
TABLE 2-41. LATTICE 7648 PEAKING .....	2-64
TABLE 2-42. LATTICE 7649 PEAKING .....	2-65
TABLE 2-43. LATTICE 7650 PEAKING .....	2-66
TABLE 2-44. LATTICE 7651 PEAKING .....	2-67
TABLE 2-45. LATTICE 7652 PEAKING .....	2-68
TABLE 2-46. LATTICE 7653 PEAKING .....	2-69
TABLE 2-47. LATTICE 7654 PEAKING .....	2-70

## LIST OF TABLES

TABLE 2-48. LATTICE 7655 PEAKING .....	2-71
TABLE 2-49. BUNDLE 2990 UNCONTROLLED AND CONTROLLED R-FACTORS .....	2-77
TABLE 2-50. BUNDLE 2991 UNCONTROLLED AND CONTROLLED R-FACTORS .....	2-78
TABLE 2-51. BUNDLE 2992 UNCONTROLLED AND CONTROLLED R-FACTORS .....	2-79
TABLE 2-52. BUNDLE 2993 UNCONTROLLED AND CONTROLLED R-FACTORS .....	2-80
TABLE 2-53. BUNDLE 2994 UNCONTROLLED AND CONTROLLED R-FACTORS .....	2-81
TABLE 2-54. LATTICE 7633 $K_{\infty}$ .....	2-87
TABLE 2-55. LATTICE 7638 $K_{\infty}$ .....	2-88
TABLE 2-56. LATTICE 7644 $K_{\infty}$ .....	2-89
TABLE 2-57. LATTICE 7648 $K_{\infty}$ .....	2-90
TABLE 2-58. LATTICE 7652 $K_{\infty}$ .....	2-91
TABLE 3-1. HOT DESIGN EIGENVALUES .....	3-11
TABLE 3-2. COLD DESIGN EIGENVALUES.....	3-12
TABLE 3-3. AXIAL NODAL POWER SEQ-1 .....	3-21
TABLE 3-4. AXIAL NODAL POWER SEQ-2.....	3-22
TABLE 3-5. AXIAL NODAL POWER SEQ-3.....	3-23
TABLE 3-6. AXIAL NODAL POWER SEQ-4.....	3-24
TABLE 3-7. AXIAL NODAL EXPOSURE SEQ-1.....	3-25
TABLE 3-8. AXIAL NODAL EXPOSURE SEQ-2.....	3-26
TABLE 3-9. AXIAL NODAL EXPOSURE SEQ-3.....	3-27
TABLE 3-10. AXIAL NODAL EXPOSURE SEQ-4.....	3-28
TABLE 3-11. HOT $K_{\text{EFF}}$ VS EXPOSURE.....	3-29
TABLE 3-12. RPF VS EXPOSURE .....	3-31
TABLE 3-13. MFLPD VS EXPOSURE .....	3-40
TABLE 3-14. MCPR VS EXPOSURE.....	3-49
TABLE 3-15. HOT EXCESS REACTIVITY .....	3-58
TABLE 3-16. COLD SHUTDOWN MARGIN .....	3-60
TABLE 3-17. SLCS SHUTDOWN MARGIN.....	3-67
TABLE 3-18. EIGENVALUES FOR CRITICAL CRP .....	3-68
TABLE 3-19. MTC FOR CRITICAL CRP.....	3-69
TABLE 3-20. EIGENVALUES FOR CRITICAL CRP .....	3-70
TABLE 3-21. MVC FOR CRITICAL CRP .....	3-71

## **Abstract**

The purpose of this report is to document the steady state nuclear characteristics of the ESBWR initial core consistent with those reported in NEDC-33239P (Reference 1) for the analysis basis equilibrium core and to demonstrate conformance with nuclear design requirements. An ESBWR reference initial core has been designed to achieve an eighteen month operating cycle utilizing the GE14E bundle. The bundle designs and core design are evaluated based on the nuclear physics methods previously described in Reference 1. Section 1 of this report summarizes the design bases that were established to develop effective designs for the ESBWR Cycle 1 bundles and core. Discussion is included on nuclear dynamic parameters, shutdown margin, overpower bases, standby liquid control system and stability bases. Section 2 presents the GE14E bundles that were designed specifically for the ESBWR initial core to achieve adequate performance. Illustrations of each bundle are provided that shows the pin-by-pin enrichment of each lattice and the axial location of each lattice within each bundle design. Reactivity and local peaking characteristics are discussed relative to core performance. Finally, the detailed core performance results are presented in Section 3. Results include hot excess reactivity, cold shutdown margin, standby liquid control system margin, a rodged depletion scenario throughout the cycle and other analysis results that describe Cycle 1 performance. This report illustrates that all nuclear design requirements as stipulated in Section 1 have been met.

## ACRONYMS AND ABBREVIATIONS

<u>Acronym</u>	<u>Description</u>
APLHGR	Average Planar Linear Heat Generation Rate
AOO	Anticipated Operational Occurrences
ARI	All Rods In
BOC	Beginning of Operating Cycle
BOL	Beginning of Life
BWR	Boiling Water Reactor
CBH	Control Blade History
CCC	Control Cell Core
CPR	Critical Power Ratio
ECCS	Emergency Core Cooling System
EFPD	Effective Full Power Days
EOC	End of Operating Cycle
ESBWR	Economic Simplified Boiling Water Reactor
GDC	General Design Criteria
HCU	Hydraulic Control Unit
HOTUNC	Hot Uncontrolled K-infinities
HOTUNC D	Hot Uncontrolled K-infinities - Doppler
LCO	Limiting Condition of Operation
LHGR	Linear Heat Generation Rate
MAPLHGR	Maximum Average Planar Linear Heat Generation Rate
MAPRAT	Ratio of APLHGR to MAPLHGR
MCPR	Minimum Critical Power Ratio
MFLCPR	Maximum Fraction of Limiting Critical Power Ratio
MFLPD	Maximum Fraction of Limiting Power Density
MLHGR	Maximum Linear Heat Generation Rate
MOC	Middle of Operating Cycle
MTC	Moderator Temperature Coefficient
MVC	Moderator Void Coefficient
OLMCPR	Operating Limit Minimum Critical Power Ratio
OLTP	Operating Licensed Thermal Power
SDM	Shutdown Margin
SLCS	Standby Liquid Control System
SRO	Strongest Rod Out

## 1. NUCLEAR DESIGN BASIS

The design bases are those that are required for the plant to operate, meeting all safety requirements. The safety design bases that are required fall into two categories:

- The reactivity basis, which prevents an uncontrolled positive reactivity excursion.
- The overpower bases for the control of power distribution, which prevent the core from operating beyond the fuel integrity limits.

This report describes how the ESBWR initial core and GE14E bundle designs conform to these design bases. The applicable General Design Criteria (GDC) as described in Appendix A of 10 CFR 50, "General Design Criteria for Nuclear Power Plants," have been identified below and are the same as those applied to the ESBWR equilibrium core design in Reference 1. All evaluation results presented herein are based on the nuclear methods that have been described in detail in Reference 1.

### 1.1 Negative Reactivity Feedback Bases

Reactivity coefficients, the differential changes in reactivity produced by differential changes in core conditions, are useful in calculating stability and evaluating the response of the core to external disturbances. The base initial condition of the system and the postulated initiating event determine which of the several defined coefficients are significant in evaluating the response of the reactor. The coefficients of interest are the Doppler coefficient, the moderator void reactivity coefficient and the moderator temperature coefficient. Also associated with the BWR is a power reactivity coefficient. The power coefficient is a combination of the Doppler and void reactivity coefficients in the power operating range; this is not explicitly evaluated. The Doppler coefficient, the moderator void reactivity coefficient and the moderator temperature coefficient of reactivity shall be negative for power operating conditions, thereby providing negative reactivity feedback characteristics. The above design basis meets GDC 11.

The Doppler coefficient, relative to the bundle nuclear design, is discussed in more detail in Section 2. The moderator temperature and void coefficients are discussed in more detail in Section 3.

### 1.2 Control Requirements (Shutdown Margins)

The core must be capable of being made sub-critical, with margin, in the most reactive condition throughout the operating cycle with the highest worth control rod, or rod pair, stuck in the full-out position and all other rods fully inserted. This design basis satisfies GDC 26. Shutdown margin (SDM) evaluation results for the ESBWR initial core design are presented in Section 3.

### 1.3 Control Requirements (Overpower Bases)

The nuclear design basis for control requirements is that the Maximum Linear Heat Generation Rate (MLHGR) and the Minimum Critical Power Ratio (MCPR) constraints shall be met during operation. The MCPR and MLHGR are determined such that, with 95% confidence, the fuel does not exceed required licensing limits during abnormal operational occurrences (AOO). This design basis satisfies GDC 10.

MLHGR and MCPR are defined as follows:

### **1.3.1 Maximum Linear Heat Generation Rate**

The MLHGR is the maximum linear heat generation for the fuel rod with the highest linear power density at a given nodal plane in the bundle. The MLHGR operating limit is bundle type dependent. The MLHGR can be monitored to assure that all thermal-mechanical design requirements are met. The fuel will not be operated at MLHGR values greater than those found to be acceptable within the body of the safety analysis under normal operating conditions. Under abnormal conditions, including the maximum overpower condition, the MLHGR will not cause fuel melting or cause the stress and strain limits to be exceeded.

### **1.3.2 Minimum Critical Power Ratio**

The MCPR is the minimum CPR allowed for a given bundle type to avoid boiling transition. The CPR is a function of several parameters; the most important of which are bundle power, bundle flow, the local power distribution and specific features of the bundle mechanical design. The plant Operating Limit MCPR (OLMCPR) is established by considering the limiting AOO for each operating cycle. The OLMCPR is determined such that 99.9% of the rods avoid boiling transition during the transient of the limiting analyzed AOO.

Detailed evaluation results including MLHGR and MCPR throughout the cycle, based on a roddeed depletion scenario, are presented in Section 3.

## **1.4 Control Requirements (Standby Liquid Control System)**

GDC 27 requires that the reactivity control systems have a combined capability, in conjunction with poison addition by the emergency core cooling system (ECCS), of reliably controlling reactivity changes under postulated accident conditions, with appropriate margin for stuck rods. The nuclear design basis is that, assuming a stuck rod, or rod pair, the standby liquid control system (SLCS) provides sufficient liquid poison into the system so that sufficient shutdown margin is achieved.

SLCS evaluation results for the ESBWR initial core design are presented in Section 3.

## **1.5 Stability Bases**

The licensing basis for stability must comply with the requirements of GDC 10 and 12.

GDC 10 (Reactor Design) requires that:

“The reactor core and associated coolant, control, and protection systems shall be designed with appropriate margin to assure that specified acceptable fuel design limits are not exceeded during any condition of normal operation, including the effects of anticipated operational occurrences.”

GDC 12 (Suppression of Reactor Power Oscillations) requires that:

“The reactor core and associated coolant, control, and protection systems shall be designed to assure that power oscillations which can result in conditions exceeding specified acceptable fuel design limits are not possible or can be reliably and readily detected and suppressed.”

Xenon stability performance is discussed in Section 3.

## 2. BUNDLE DESIGN EVALUATION

### 2.1 Introduction

Bundle and lattice designs have been developed using the methodology and codes described in Reference 1. This section presents several GE14E bundles that have been designed for initial core operation. Given that core operation begins from zero exposure conditions, multiple designs are needed to achieve the desired distribution of power in both radial and axial directions, thereby meeting the key design bases discussed in Section 1.

### 2.2 Bundle and Lattice Designs

A total of five unique GE14E bundle designs have been developed for the ESBWR reference initial core. Each bundle design is comprised of several unique lattice configurations as shown in the table below. The bundle designs are described in Figures 2-1 through 2-20. These figures include the 2-D pin-by-pin enrichment array for each lattice, axial profiles for each unique rod type, the axial location of each lattice within the bundle and the splits and weights for each bundle.

Bundle Number	Bundle Name	Number of Lattices	Lattice Numbers
2990	[[		
2991			
2992			
2993			
2994			]]

Many factors are considered in the development of these bundle designs in addition to overall cycle energy requirements and operating strategy. Perhaps the key considerations are given to achieving the desired reactivity and local peaking behavior required for an initial core application. Acceptability of the designs can be confirmed when the overall performance is assessed by 3-D simulator evaluations using the methodology and codes discussed in Reference 1. Lattice reactivity characteristics can be judged by the core hot excess reactivity and cold shutdown margin behavior. Lattice k-infinities versus burn-up for the hot uncontrolled condition at three void history fractions have been provided in Tables 2-1 through 2-24 and in Figures 2-21 through 2-44 for each lattice design. Similarly, lattice local peaking characteristics can be judged by the thermal margin performance as determined by 3-D simulator calculations. The maximum lattice local peaking versus burn-up for the hot uncontrolled condition at the same void history fractions are provided in Tables 2-25 through 2-48 and in Figures 2-45 through 2-68 for each lattice design. Core reactivity and thermal margin performance results based on these bundle designs will be presented in Section 3. Acceptable core performance is strongly dependent on the k-infinity and local peaking characteristics at the bundle and lattice design level.

### 2.2.1 GE14E Bundle Design Features for Initial Core

As previously mentioned, each GE14E bundle designed for this initial core application consists of several unique lattice configurations. The top and bottom lattice of each bundle consists of a six inch blanket of natural uranium. The first enriched lattice above the bottom natural uranium zone is referred to as the "dominant" zone. This lattice represents the largest zone within the bundle and establishes the overall reactivity characteristics. For reload applications, the GE14E design may include a shorter power shaping zone as the first enriched zone at the bottom. However, for an initial core application in which all bundles have zero burn-up history, such a zone is not necessary. The remaining lattices above the dominant zone correctly model the axially varying geometry (i.e., plenums and vanishing rods) that is associated with the part length rod feature of the GE14E design.

### 2.2.2 Bundle Local Peaking

One of the important parameters affecting linear heat generation rate (LHGR) performance of a bundle is the local peaking value. Figures 2-69 through 2-73 provide the 2-D pin-by-pin lattice local peaking values for each dominant lattice of all bundle designs at 40% void and beginning of life (BOL) conditions. This is in addition to the maximum lattice local peaking versus burn-up data previously provided. The resulting core LHGR performance based on a roddepleted depletion scenario is described in Section 3.

### 2.2.3 Bundle R-Factor

An important parameter affecting the critical power performance of a BWR is the exposure dependent bundle R-factor. Table 2-49 through 2-53 shows the fully uncontrolled and fully controlled R-factors for zero mils channel bow as a function of burn-up for all initial core bundle designs. To further illustrate how these maximum values are derived, the 2-D pin-by-pin R-factors for each bundle are shown in Figures 2-74 through 2-78 at 20 GWd/ST for the fully uncontrolled condition and zero mils channel bow. In general, the bundle design for an ESBWR attempts to achieve optimum thermal margins (i.e., MLHGR and MCPR) by minimizing local peaking and R-factors. The resulting core MCPR performance based on a roddepleted depletion scenario is described in Section 3.

### 2.2.4 Doppler Reactivity Coefficient

The Doppler coefficient is a measure of the reactivity change associated with an increase in the absorption of resonance-energy neutrons caused by a change in the temperature of the material in question. The Doppler reactivity coefficient provides instantaneous negative reactivity feedback to any rise in fuel temperature, on either a gross or local basis. The magnitude of the Doppler coefficient is inherent in the fuel design and does not vary significantly among BWR designs. For most structural and moderator materials, resonance absorption is not significant, but in  $U^{238}$  and  $Pu^{240}$  an increase in temperature produces a comparatively large increase in the effective absorption cross-section. The resulting parasitic absorption of neutrons causes an immediate loss in reactivity.

A demonstration of this can be found by observing the k-infinities at nominal and elevated fuel temperature for the dominant lattices of each ESBWR initial core GE14E bundle design. Figure



2-79 through Figure 2-83 illustrate the hot uncontrolled k-infinities for the dominant lattice at 40% voids. The k-infinity data is also provided in Tables 2-54 through 2-58 (note "HOTUNCD" indicates k-infinity data at elevated fuel temperature). For all figures, the effects of Doppler [[ ]]. This trend is expected and consistent for all ESBWR lattices within all reference designs.

A discussion on the Doppler reactivity coefficient was provided in Section 1 of Reference 1. A parameter labeled CDOP was introduced to characterize this reactivity coefficient:

$$CDOP = \frac{1000(k_{T_1} - k_{T_0})}{k_{T_0}(\sqrt{T_1} - \sqrt{T_0})}$$

where:

- $T_0$  = normal hot operating temperature (Kelvin).
- $T_1$  = elevated temperature (Kelvin).
- $k_{T_1}$  = eigenvalue at elevated temperature.
- $k_{T_0}$  = eigenvalue at normal operating temperature.

The CDOP values were determined for the ESBWR GE14E initial core. For all cases evaluated, the CDOP value was found to be negative. Typical values for the lattices found in the initial core GE14E bundles range from about [[ ]]. This compares to a typical CDOP value of [[ ]] that was reported in Reference 2 for GE14 compliance to Amendment 22. This is expected given the lower  $U^{235}$  enrichments of the initial core bundles.

### 2.3 Summary

This section described five GE14E bundle nuclear designs that have been developed to meet all nuclear design bases presented in Section 1. These bundles are intended for an initial core application. Detailed core performance results utilizing these designs are presented in Section 3.

[[

]]

**Figure 2-1. Bundle Design for 2990**

[[

]]

**Figure 2-2. Fuel Rods for 2990**

[[ ]]

**Figure 2-3. Fuel Rods for 2990**

[[

]]

**Figure 2-4. Splits and Weights for 2990**

[[

]]

**Figure 2-5. Bundle Design for 2991**

[[

]]

**Figure 2-6. Fuel Rods for 2991**

[[

]]

**Figure 2-7. Fuel Rods for 2991**



[[

]]

**Figure 2-8. Splits and Weights for 2991**

[[

]]

**Figure 2-9. Bundle Design for 2992**

[[

]]

**Figure 2-10. Fuel Rods for 2992**

[[

]]

**Figure 2-11. Fuel Rods for 2992**

[[

]]

**Figure 2-12. Splits and Weights for 2992**

[[

]]

**Figure 2-13. Bundle Design for 2993**

[[

]]

**Figure 2-14. Fuel Rods for 2993**

[[ ]]

**Figure 2-15. Fuel Rods for 2993**



[[

]]

**Figure 2-16. Splits and Weights for 2993**

[[

]]

**Figure 2-17. Bundle Design for 2994**

[[

]]

**Figure 2-18. Fuel Rods for 2994**

[[

]]

**Figure 2-19. Fuel Rods for 2994**

[[

]]

**Figure 2-20. Splits and Weights for 2994**

**Table 2-1. Lattice 7632 K-infinity**

Exposure (GWd/ST)	K-infinity		
	VF 0.0	VF 0.4	VF 0.7
0.0	[[		
0.2			
1.0			
2.0			
3.0			
4.0			
5.0			
6.0			
7.0			
8.0			
9.0			
10.0			
11.0			
12.0			
13.0			
14.0			
15.0			
16.0			
17.0			
18.0			
19.0			
20.0			
21.0			
22.0			
23.0			
24.0			
25.0			
30.0			
35.0			
40.0			
45.0			
50.0			
55.0			
60.0			
65.0			]]

[[

]]

**Figure 2-21. Lattice 7632 K-infinity**

(\* K-infinity based on three void history fractions of 0.0, 0.4 and 0.7)

**Table 2-2. Lattice 7633 K-infinity**

Exposure (GWd/ST)	K-infinity		
	VF 0.0	VF 0.4	VF 0.7
0.0	[[		
0.2			
1.0			
2.0			
3.0			
4.0			
5.0			
6.0			
7.0			
8.0			
9.0			
10.0			
11.0			
12.0			
13.0			
14.0			
15.0			
16.0			
17.0			
18.0			
19.0			
20.0			
21.0			
22.0			
23.0			
24.0			
25.0			
30.0			
35.0			
40.0			
45.0			
50.0			
55.0			
60.0			
65.0			]]

[[

]]

**Figure 2-22. Lattice 7633 K-infinity**

(\* K-infinity based on three void history fractions of 0.0, 0.4 and 0.7)

Table 2-3. Lattice 7634 K-infinity

Exposure (GWd/ST)	K-infinity		
	VF 0.0	VF 0.4	VF 0.7
0.0	[[		
0.2			
1.0			
2.0			
3.0			
4.0			
5.0			
6.0			
7.0			
8.0			
9.0			
10.0			
11.0			
12.0			
13.0			
14.0			
15.0			
16.0			
17.0			
18.0			
19.0			
20.0			
21.0			
22.0			
23.0			
24.0			
25.0			
30.0			
35.0			
40.0			
45.0			
50.0			
55.0			
60.0			
65.0			]]

[[

]]

Figure 2-23. Lattice 7634 K-infinity

(\* K-infinity based on three void history fractions of 0.0, 0.4 and 0.7)



Table 2-4. Lattice 7635 K-infinity

Exposure (GWd/ST)	K-infinity		
	VF 0.0	VF 0.4	VF 0.7
0.0	[[		
0.2			
1.0			
2.0			
3.0			
4.0			
5.0			
6.0			
7.0			
8.0			
9.0			
10.0			
11.0			
12.0			
13.0			
14.0			
15.0			
16.0			
17.0			
18.0			
19.0			
20.0			
21.0			
22.0			
23.0			
24.0			
25.0			
30.0			
35.0			
40.0			
45.0			
50.0			
55.0			
60.0			
65.0			]]

[[

]]

Figure 2-24. Lattice 7635 K-infinity

(\* K-infinity based on three void history fractions of 0.0, 0.4 and 0.7)

**Table 2-5. Lattice 7636 K-infinity**

Exposure (GWd/ST)	K-infinity		
	VF 0.0	VF 0.4	VF 0.7
0.0	[[		
0.2			
1.0			
2.0			
3.0			
4.0			
5.0			
6.0			
7.0			
8.0			
9.0			
10.0			
11.0			
12.0			
13.0			
14.0			
15.0			
16.0			
17.0			
18.0			
19.0			
20.0			
21.0			
22.0			
23.0			
24.0			
25.0			
30.0			
35.0			
40.0			
45.0			
50.0			
55.0			
60.0			
65.0			]]

[[

]]

**Figure 2-25. Lattice 7636 K-infinity**

(\* K-infinity based on three void history fractions of 0.0, 0.4 and 0.7)

Table 2-6. Lattice 7637 K-infinity

Exposure (GWd/ST)	K-infinity		
	VF 0.0	VF 0.4	VF 0.7
0.0	[[		
0.2			
1.0			
2.0			
3.0			
4.0			
5.0			
6.0			
7.0			
8.0			
9.0			
10.0			
11.0			
12.0			
13.0			
14.0			
15.0			
16.0			
17.0			
18.0			
19.0			
20.0			
21.0			
22.0			
23.0			
24.0			
25.0			
30.0			
35.0			
40.0			
45.0			
50.0			
55.0			
60.0			
65.0			]]

[[

]]

Figure 2-26. Lattice 7637 K-infinity

(\* K-infinity based on three void history fractions of 0.0, 0.4 and 0.7)

Table 2-7. Lattice 7638 K-infinity

Exposure (GWd/ST)	K-infinity		
	VF 0.0	VF 0.4	VF 0.7
0.0	[[		
0.2			
1.0			
2.0			
3.0			
4.0			
5.0			
6.0			
7.0			
8.0			
9.0			
10.0			
11.0			
12.0			
13.0			
14.0			
15.0			
16.0			
17.0			
18.0			
19.0			
20.0			
21.0			
22.0			
23.0			
24.0			
25.0			
30.0			
35.0			
40.0			
45.0			
50.0			
55.0			
60.0			
65.0			]]

[[

]]

Figure 2-27. Lattice 7638 K-infinity

(\* K-infinity based on three void history fractions of 0.0, 0.4 and 0.7)

**Table 2-8. Lattice 7639 K-infinity**

Exposure (GWd/ST)	K-infinity		
	VF 0.0	VF 0.4	VF 0.7
0.0	[[		
0.2			
1.0			
2.0			
3.0			
4.0			
5.0			
6.0			
7.0			
8.0			
9.0			
10.0			
11.0			
12.0			
13.0			
14.0			
15.0			
16.0			
17.0			
18.0			
19.0			
20.0			
21.0			
22.0			
23.0			
24.0			
25.0			
30.0			
35.0			
40.0			
45.0			
50.0			
55.0			
60.0			
65.0			]]

[[

]]

**Figure 2-28. Lattice 7639 K-infinity**

(\* K-infinity based on three void history fractions of 0.0, 0.4 and 0.7)

**Table 2-9. Lattice 7640 K-infinity**

Exposure (GWd/ST)	K-infinity		
	VF 0.0	VF 0.4	VF 0.7
0.0	[[		
0.2			
1.0			
2.0			
3.0			
4.0			
5.0			
6.0			
7.0			
8.0			
9.0			
10.0			
11.0			
12.0			
13.0			
14.0			
15.0			
16.0			
17.0			
18.0			
19.0			
20.0			
21.0			
22.0			
23.0			
24.0			
25.0			
30.0			
35.0			
40.0			
45.0			
50.0			
55.0			
60.0			
65.0			]]

[[

]]

**Figure 2-29. Lattice 7640 K-infinity**

(\* K-infinity based on three void history fractions of 0.0, 0.4 and 0.7)

**Table 2-10. Lattice 7641 K-infinity**

Exposure (GWd/ST)	K-infinity		
	VF 0.0	VF 0.4	VF 0.7
0.0	[[		
0.2			
1.0			
2.0			
3.0			
4.0			
5.0			
6.0			
7.0			
8.0			
9.0			
10.0			
11.0			
12.0			
13.0			
14.0			
15.0			
16.0			
17.0			
18.0			
19.0			
20.0			
21.0			
22.0			
23.0			
24.0			
25.0			
30.0			
35.0			
40.0			
45.0			
50.0			
55.0			
60.0			
65.0			]]

[[

]]

**Figure 2-30. Lattice 7641 K-infinity**

(\* K-infinity based on three void history fractions of 0.0, 0.4 and 0.7)

**Table 2-11. Lattice 7642 K-infinity**

Exposure (GWd/ST)	K-infinity		
	VF 0.0	VF 0.4	VF 0.7
0.0	[[		
0.2			
1.0			
2.0			
3.0			
4.0			
5.0			
6.0			
7.0			
8.0			
9.0			
10.0			
11.0			
12.0			
13.0			
14.0			
15.0			
16.0			
17.0			
18.0			
19.0			
20.0			
21.0			
22.0			
23.0			
24.0			
25.0			
30.0			
35.0			
40.0			
45.0			
50.0			
55.0			
60.0			
65.0			]]

[[

]]

**Figure 2-31. Lattice 7642 K-infinity**

(\* K-infinity based on three void history fractions of 0.0, 0.4 and 0.7)



Table 2-12. Lattice 7643 K-infinity

Exposure (Gwd/ST)	K-infinity		
	VF 0.0	VF 0.4	VF 0.7
0.0	[[		
0.2			
1.0			
2.0			
3.0			
4.0			
5.0			
6.0			
7.0			
8.0			
9.0			
10.0			
11.0			
12.0			
13.0			
14.0			
15.0			
16.0			
17.0			
18.0			
19.0			
20.0			
21.0			
22.0			
23.0			
24.0			
25.0			
30.0			
35.0			
40.0			
45.0			
50.0			
55.0			
60.0			
65.0			]]

[[

]]

Figure 2-32. Lattice 7643 K-infinity

(\* K-infinity based on three void history fractions of 0.0, 0.4 and 0.7)

Table 2-13. Lattice 7644 K-infinity

Exposure (GWd/ST)	K-infinity		
	VF 0.0	VF 0.4	VF 0.7
0.0	[[		
0.2			
1.0			
2.0			
3.0			
4.0			
5.0			
6.0			
7.0			
8.0			
9.0			
10.0			
11.0			
12.0			
13.0			
14.0			
15.0			
16.0			
17.0			
18.0			
19.0			
20.0			
21.0			
22.0			
23.0			
24.0			
25.0			
30.0			
35.0			
40.0			
45.0			
50.0			
55.0			
60.0			
65.0			]]

[[

]]

Figure 2-33. Lattice 7644 K-infinity

(\* K-infinity based on three void history fractions of 0.0, 0.4 and 0.7)

Table 2-14. Lattice 7645 K-infinity

Exposure (GWd/ST)	K-infinity		
	VF 0.0	VF 0.4	VF 0.7
0.0	[[		
0.2			
1.0			
2.0			
3.0			
4.0			
5.0			
6.0			
7.0			
8.0			
9.0			
10.0			
11.0			
12.0			
13.0			
14.0			
15.0			
16.0			
17.0			
18.0			
19.0			
20.0			
21.0			
22.0			
23.0			
24.0			
25.0			
30.0			
35.0			
40.0			
45.0			
50.0			
55.0			
60.0			
65.0			]]

[[

]]

Figure 2-34. Lattice 7645 K-infinity

(\* K-infinity based on three void history fractions of 0.0, 0.4 and 0.7)

Table 2-15. Lattice 7646 K-infinity

Exposure (GWd/ST)	K-infinity		
	VF 0.0	VF 0.4	VF 0.7
0.0	[[		
0.2			
1.0			
2.0			
3.0			
4.0			
5.0			
6.0			
7.0			
8.0			
9.0			
10.0			
11.0			
12.0			
13.0			
14.0			
15.0			
16.0			
17.0			
18.0			
19.0			
20.0			
21.0			
22.0			
23.0			
24.0			
25.0			
30.0			
35.0			
40.0			
45.0			
50.0			
55.0			
60.0			
65.0			]]

[[

]]

Figure 2-35. Lattice 7646 K-infinity

(\* K-infinity based on three void history fractions of 0.0, 0.4 and 0.7)

Table 2-16. Lattice 7647 K-infinity

Exposure (GWd/ST)	K-infinity		
	VF 0.0	VF 0.4	VF 0.7
0.0	[[		
0.2			
1.0			
2.0			
3.0			
4.0			
5.0			
6.0			
7.0			
8.0			
9.0			
10.0			
11.0			
12.0			
13.0			
14.0			
15.0			
16.0			
17.0			
18.0			
19.0			
20.0			
21.0			
22.0			
23.0			
24.0			
25.0			
30.0			
35.0			
40.0			
45.0			
50.0			
55.0			
60.0			
65.0			]]

[[

]]

Figure 2-36. Lattice 7647 K-infinity

(\* K-infinity based on three void history fractions of 0.0, 0.4 and 0.7)

Table 2-17. Lattice 7648 K-infinity

Exposure (GWd/ST)	K-infinity		
	VF 0.0	VF 0.4	VF 0.7
0.0	[[		
0.2			
1.0			
2.0			
3.0			
4.0			
5.0			
6.0			
7.0			
8.0			
9.0			
10.0			
11.0			
12.0			
13.0			
14.0			
15.0			
16.0			
17.0			
18.0			
19.0			
20.0			
21.0			
22.0			
23.0			
24.0			
25.0			
30.0			
35.0			
40.0			
45.0			
50.0			
55.0			
60.0			
65.0			]]

[[

]]

Figure 2-37. Lattice 7648 K-infinity

(\* K-infinity based on three void history fractions of 0.0, 0.4 and 0.7)

**Table 2-18. Lattice 7649 K-infinity**

Exposure (GWd/ST)	K-infinity		
	VF 0.0	VF 0.4	VF 0.7
0.0	[[		
0.2			
1.0			
2.0			
3.0			
4.0			
5.0			
6.0			
7.0			
8.0			
9.0			
10.0			
11.0			
12.0			
13.0			
14.0			
15.0			
16.0			
17.0			
18.0			
19.0			
20.0			
21.0			
22.0			
23.0			
24.0			
25.0			
30.0			
35.0			
40.0			
45.0			
50.0			
55.0			
60.0			
65.0			]]

[[

]]

**Figure 2-38. Lattice 7649 K-infinity**

(\* K-infinity based on three void history fractions of 0.0, 0.4 and 0.7)

**Table 2-19. Lattice 7650 K-infinity**

Exposure (Gwd/ST)	K-infinity		
	VF 0.0	VF 0.4	VF 0.7
0.0	[[		
0.2			
1.0			
2.0			
3.0			
4.0			
5.0			
6.0			
7.0			
8.0			
9.0			
10.0			
11.0			
12.0			
13.0			
14.0			
15.0			
16.0			
17.0			
18.0			
19.0			
20.0			
21.0			
22.0			
23.0			
24.0			
25.0			
30.0			
35.0			
40.0			
45.0			
50.0			
55.0			
60.0			
65.0			]]

[[

]]

**Figure 2-39. Lattice 7650 K-infinity**

(\* K-infinity based on three void history fractions of 0.0, 0.4 and 0.7)



Table 2-20. Lattice 7651 K-infinity

Exposure (GWd/ST)	K-infinity		
	VF 0.0	VF 0.4	VF 0.7
0.0	[[		
0.2			
1.0			
2.0			
3.0			
4.0			
5.0			
6.0			
7.0			
8.0			
9.0			
10.0			
11.0			
12.0			
13.0			
14.0			
15.0			
16.0			
17.0			
18.0			
19.0			
20.0			
21.0			
22.0			
23.0			
24.0			
25.0			
30.0			
35.0			
40.0			
45.0			
50.0			
55.0			
60.0			
65.0			]]

[[

]]

Figure 2-40. Lattice 7651 K-infinity

(\* K-infinity based on three void history fractions of 0.0, 0.4 and 0.7)

**Table 2-21. Lattice 7652 K-infinity**

Exposure (GWd/ST)	K-infinity		
	VF 0.0	VF 0.4	VF 0.7
0.0	[[		
0.2			
1.0			
2.0			
3.0			
4.0			
5.0			
6.0			
7.0			
8.0			
9.0			
10.0			
11.0			
12.0			
13.0			
14.0			
15.0			
16.0			
17.0			
18.0			
19.0			
20.0			
21.0			
22.0			
23.0			
24.0			
25.0			
30.0			
35.0			
40.0			
45.0			
50.0			
55.0			
60.0			
65.0			]]

[[

]]

**Figure 2-41. Lattice 7652 K-infinity**

(\* K-infinity based on three void history fractions of 0.0, 0.4 and 0.7)

Table 2-22. Lattice 7653 K-infinity

Exposure (GWd/ST)	K-infinity		
	VF 0.0	VF 0.4	VF 0.7
0.0	[[		
0.2			
1.0			
2.0			
3.0			
4.0			
5.0			
6.0			
7.0			
8.0			
9.0			
10.0			
11.0			
12.0			
13.0			
14.0			
15.0			
16.0			
17.0			
18.0			
19.0			
20.0			
21.0			
22.0			
23.0			
24.0			
25.0			
30.0			
35.0			
40.0			
45.0			
50.0			
55.0			
60.0			
65.0			]]

[[

]]

Figure 2-42. Lattice 7653 K-infinity

(\* K-infinity based on three void history fractions of 0.0, 0.4 and 0.7)

**Table 2-23. Lattice 7654 K-infinity**

Exposure (GWd/ST)	K-infinity		
	VF 0.0	VF 0.4	VF 0.7
0.0	[[		
0.2			
1.0			
2.0			
3.0			
4.0			
5.0			
6.0			
7.0			
8.0			
9.0			
10.0			
11.0			
12.0			
13.0			
14.0			
15.0			
16.0			
17.0			
18.0			
19.0			
20.0			
21.0			
22.0			
23.0			
24.0			
25.0			
30.0			
35.0			
40.0			
45.0			
50.0			
55.0			
60.0			
65.0			]]

[[

]]

**Figure 2-43. Lattice 7654 K-infinity**

(\* K-infinity based on three void history fractions of 0.0, 0.4 and 0.7)

Table 2-24. Lattice 7655 K-infinity

Exposure (GWd/ST)	K-infinity		
	VF 0.0	VF 0.4	VF 0.7
0.0	[[		
0.2			
1.0			
2.0			
3.0			
4.0			
5.0			
6.0			
7.0			
8.0			
9.0			
10.0			
11.0			
12.0			
13.0			
14.0			
15.0			
16.0			
17.0			
18.0			
19.0			
20.0			
21.0			
22.0			
23.0			
24.0			
25.0			
30.0			
35.0			
40.0			
45.0			
50.0			
55.0			
60.0			
65.0			]]

[[

]]

Figure 2-44. Lattice 7655 K-infinity

(\* K-infinity based on three void history fractions of 0.0, 0.4 and 0.7)

Table 2-25. Lattice 7632 Peaking

Exposure (GWd/ST)	Maximum Local Peaking		
	VF 0.0	VF 0.4	VF 0.7
0.0	[[		
0.2			
1.0			
2.0			
3.0			
4.0			
5.0			
6.0			
7.0			
8.0			
9.0			
10.0			
11.0			
12.0			
13.0			
14.0			
15.0			
16.0			
17.0			
18.0			
19.0			
20.0			
21.0			
22.0			
23.0			
24.0			
25.0			
30.0			
35.0			
40.0			
45.0			
50.0			
55.0			
60.0			
65.0			]]

[[

]]

Figure 2-45. Lattice 7632 Maximum Local Peaking

(\* Local peaking based on three void history fractions of 0.0, 0.4 and 0.7)

**Table 2-26. Lattice 7633 Peaking**

<b>Exposure (GWd/ST)</b>	<b>Maximum Local Peaking</b>		
	<b>VF 0.0</b>	<b>VF 0.4</b>	<b>VF 0.7</b>
0.0	[[		
0.2			
1.0			
2.0			
3.0			
4.0			
5.0			
6.0			
7.0			
8.0			
9.0			
10.0			
11.0			
12.0			
13.0			
14.0			
15.0			
16.0			
17.0			
18.0			
19.0			
20.0			
21.0			
22.0			
23.0			
24.0			
25.0			
30.0			
35.0			
40.0			
45.0			
50.0			
55.0			
60.0			
65.0			]]

[[

]]

**Figure 2-46. Lattice 7633 Maximum Local Peaking**

(\* Local peaking based on three void history fractions of 0.0, 0.4 and 0.7)

**Table 2-27. Lattice 7634 Peaking**

<b>Exposure (GWd/ST)</b>	<b>Maximum Local Peaking</b>		
	<b>VF 0.0</b>	<b>VF 0.4</b>	<b>VF 0.7</b>
0.0	[[		
0.2			
1.0			
2.0			
3.0			
4.0			
5.0			
6.0			
7.0			
8.0			
9.0			
10.0			
11.0			
12.0			
13.0			
14.0			
15.0			
16.0			
17.0			
18.0			
19.0			
20.0			
21.0			
22.0			
23.0			
24.0			
25.0			
30.0			
35.0			
40.0			
45.0			
50.0			
55.0			
60.0			
65.0			]]

[[

]]

**Figure 2-47. Lattice 7634 Maximum Local Peaking**

(\* Local peaking based on three void history fractions of 0.0, 0.4 and 0.7)



**Table 2-28. Lattice 7635 Peaking**

Exposure (GWd/ST)	Maximum Local Peaking		
	VF 0.0	VF 0.4	VF 0.7
0.0	[[		
0.2			
1.0			
2.0			
3.0			
4.0			
5.0			
6.0			
7.0			
8.0			
9.0			
10.0			
11.0			
12.0			
13.0			
14.0			
15.0			
16.0			
17.0			
18.0			
19.0			
20.0			
21.0			
22.0			
23.0			
24.0			
25.0			
30.0			
35.0			
40.0			
45.0			
50.0			
55.0			
60.0			
65.0			]]

[[

]]

**Figure 2-48. Lattice 7635 Maximum Local Peaking**

(\* Local peaking based on three void history fractions of 0.0, 0.4 and 0.7)

**Table 2-29. Lattice 7636 Peaking**

Exposure (GWd/ST)	Maximum Local Peaking		
	VF 0.0	VF 0.4	VF 0.7
0.0	[[		
0.2			
1.0			
2.0			
3.0			
4.0			
5.0			
6.0			
7.0			
8.0			
9.0			
10.0			
11.0			
12.0			
13.0			
14.0			
15.0			
16.0			
17.0			
18.0			
19.0			
20.0			
21.0			
22.0			
23.0			
24.0			
25.0			
30.0			
35.0			
40.0			
45.0			
50.0			
55.0			
60.0			
65.0			]]

[[

]]

**Figure 2-49. Lattice 7636 Maximum Local Peaking**

(\* Local peaking based on three void history fractions of 0.0, 0.4 and 0.7)

**Table 2-30. Lattice 7637 Peaking**

Exposure (GWd/ST)	Maximum Local Peaking		
	VF 0.0	VF 0.4	VF 0.7
0.0	[[		
0.2			
1.0			
2.0			
3.0			
4.0			
5.0			
6.0			
7.0			
8.0			
9.0			
10.0			
11.0			
12.0			
13.0			
14.0			
15.0			
16.0			
17.0			
18.0			
19.0			
20.0			
21.0			
22.0			
23.0			
24.0			
25.0			
30.0			
35.0			
40.0			
45.0			
50.0			
55.0			
60.0			
65.0			]]

[[

]]

**Figure 2-50. Lattice 7637 Maximum Local Peaking**

(\* Local peaking based on three void history fractions of 0.0, 0.4 and 0.7)

**Table 2-31. Lattice 7638 Peaking**

Exposure (GWd/ST)	Maximum Local Peaking		
	VF 0.0	VF 0.4	VF 0.7
0.0	[[		
0.2			
1.0			
2.0			
3.0			
4.0			
5.0			
6.0			
7.0			
8.0			
9.0			
10.0			
11.0			
12.0			
13.0			
14.0			
15.0			
16.0			
17.0			
18.0			
19.0			
20.0			
21.0			
22.0			
23.0			
24.0			
25.0			
30.0			
35.0			
40.0			
45.0			
50.0			
55.0			
60.0			
65.0			]]

[[

]]

**Figure 2-51. Lattice 7638 Maximum Local Peaking**

(\* Local peaking based on three void history fractions of 0.0, 0.4 and 0.7)

**Table 2-32. Lattice 7639 Peaking**

Exposure (GWd/ST)	Maximum Local Peaking		
	VF 0.0	VF 0.4	VF 0.7
0.0	[[		
0.2			
1.0			
2.0			
3.0			
4.0			
5.0			
6.0			
7.0			
8.0			
9.0			
10.0			
11.0			
12.0			
13.0			
14.0			
15.0			
16.0			
17.0			
18.0			
19.0			
20.0			
21.0			
22.0			
23.0			
24.0			
25.0			
30.0			
35.0			
40.0			
45.0			
50.0			
55.0			
60.0			
65.0			]]

[[

]]

**Figure 2-52. Lattice 7639 Maximum Local Peaking**

(\* Local peaking based on three void history fractions of 0.0, 0.4 and 0.7)

**Table 2-33. Lattice 7640 Peaking**

Exposure (GWd/ST)	Maximum Local Peaking		
	VF 0.0	VF 0.4	VF 0.7
0.0	[[		
0.2			
1.0			
2.0			
3.0			
4.0			
5.0			
6.0			
7.0			
8.0			
9.0			
10.0			
11.0			
12.0			
13.0			
14.0			
15.0			
16.0			
17.0			
18.0			
19.0			
20.0			
21.0			
22.0			
23.0			
24.0			
25.0			
30.0			
35.0			
40.0			
45.0			
50.0			
55.0			
60.0			
65.0			]]

[[

]]

**Figure 2-53. Lattice 7640 Maximum Local Peaking**

(\* Local peaking based on three void history fractions of 0.0, 0.4 and 0.7)

**Table 2-34. Lattice 7641 Peaking**

Exposure (GWd/ST)	Maximum Local Peaking		
	VF 0.0	VF 0.4	VF 0.7
0.0	[[		
0.2			
1.0			
2.0			
3.0			
4.0			
5.0			
6.0			
7.0			
8.0			
9.0			
10.0			
11.0			
12.0			
13.0			
14.0			
15.0			
16.0			
17.0			
18.0			
19.0			
20.0			
21.0			
22.0			
23.0			
24.0			
25.0			
30.0			
35.0			
40.0			
45.0			
50.0			
55.0			
60.0			
65.0			]]

[[

]]

**Figure 2-54. Lattice 7641 Maximum Local Peaking**

(\* Local peaking based on three void history fractions of 0.0, 0.4 and 0.7)

**Table 2-35. Lattice 7642 Peaking**

Exposure (Gwd/ST)	Maximum Local Peaking		
	VF 0.0	VF 0.4	VF 0.7
0.0	[[		
0.2			
1.0			
2.0			
3.0			
4.0			
5.0			
6.0			
7.0			
8.0			
9.0			
10.0			
11.0			
12.0			
13.0			
14.0			
15.0			
16.0			
17.0			
18.0			
19.0			
20.0			
21.0			
22.0			
23.0			
24.0			
25.0			
30.0			
35.0			
40.0			
45.0			
50.0			
55.0			
60.0			
65.0			]]

[[

]]

**Figure 2-55. Lattice 7642 Maximum Local Peaking**

(\* Local peaking based on three void history fractions of 0.0, 0.4 and 0.7)



**Table 2-36. Lattice 7643 Peaking**

Exposure (GWd/ST)	Maximum Local Peaking		
	VF 0.0	VF 0.4	VF 0.7
0.0	[[		
0.2			
1.0			
2.0			
3.0			
4.0			
5.0			
6.0			
7.0			
8.0			
9.0			
10.0			
11.0			
12.0			
13.0			
14.0			
15.0			
16.0			
17.0			
18.0			
19.0			
20.0			
21.0			
22.0			
23.0			
24.0			
25.0			
30.0			
35.0			
40.0			
45.0			
50.0			
55.0			
60.0			
65.0			]]

[[

]]

**Figure 2-56. Lattice 7643 Maximum Local Peaking**

(\* Local peaking based on three void history fractions of 0.0, 0.4 and 0.7)

**Table 2-37. Lattice 7644 Peaking**

Exposure (GWd/ST)	Maximum Local Peaking		
	VF 0.0	VF 0.4	VF 0.7
0.0	[[		
0.2			
1.0			
2.0			
3.0			
4.0			
5.0			
6.0			
7.0			
8.0			
9.0			
10.0			
11.0			
12.0			
13.0			
14.0			
15.0			
16.0			
17.0			
18.0			
19.0			
20.0			
21.0			
22.0			
23.0			
24.0			
25.0			
30.0			
35.0			
40.0			
45.0			
50.0			
55.0			
60.0			
65.0			]]

[[

]]

**Figure 2-57. Lattice 7644 Maximum Local Peaking**

(\* Local peaking based on three void history fractions of 0.0, 0.4 and 0.7)

**Table 2-38. Lattice 7645 Peaking**

Exposure (GWd/ST)	Maximum Local Peaking		
	VF 0.0	VF 0.4	VF 0.7
0.0	[[		
0.2			
1.0			
2.0			
3.0			
4.0			
5.0			
6.0			
7.0			
8.0			
9.0			
10.0			
11.0			
12.0			
13.0			
14.0			
15.0			
16.0			
17.0			
18.0			
19.0			
20.0			
21.0			
22.0			
23.0			
24.0			
25.0			
30.0			
35.0			
40.0			
45.0			
50.0			
55.0			
60.0			
65.0			]]

[[

]]

**Figure 2-58. Lattice 7645 Maximum Local Peaking**

(\* Local peaking based on three void history fractions of 0.0, 0.4 and 0.7)

**Table 2-39. Lattice 7646 Peaking**

Exposure (GWd/ST)	Maximum Local Peaking		
	VF 0.0	VF 0.4	VF 0.7
0.0	[[		
0.2			
1.0			
2.0			
3.0			
4.0			
5.0			
6.0			
7.0			
8.0			
9.0			
10.0			
11.0			
12.0			
13.0			
14.0			
15.0			
16.0			
17.0			
18.0			
19.0			
20.0			
21.0			
22.0			
23.0			
24.0			
25.0			
30.0			
35.0			
40.0			
45.0			
50.0			
55.0			
60.0			
65.0			]]

[[

]]

**Figure 2-59. Lattice 7646 Maximum Local Peaking**

(\* Local peaking based on three void history fractions of 0.0, 0.4 and 0.7)

**Table 2-40. Lattice 7647 Peaking**

Exposure (GWd/ST)	Maximum Local Peaking		
	VF 0.0	VF 0.4	VF 0.7
0.0	[[		
0.2			
1.0			
2.0			
3.0			
4.0			
5.0			
6.0			
7.0			
8.0			
9.0			
10.0			
11.0			
12.0			
13.0			
14.0			
15.0			
16.0			
17.0			
18.0			
19.0			
20.0			
21.0			
22.0			
23.0			
24.0			
25.0			
30.0			
35.0			
40.0			
45.0			
50.0			
55.0			
60.0			
65.0			]]

[[

]]

**Figure 2-60. Lattice 7647 Maximum Local Peaking**

(\* Local peaking based on three void history fractions of 0.0, 0.4 and 0.7)

**Table 2-41. Lattice 7648 Peaking**

Exposure (GWd/ST)	Maximum Local Peaking		
	VF 0.0	VF 0.4	VF 0.7
0.0	[[		
0.2			
1.0			
2.0			
3.0			
4.0			
5.0			
6.0			
7.0			
8.0			
9.0			
10.0			
11.0			
12.0			
13.0			
14.0			
15.0			
16.0			
17.0			
18.0			
19.0			
20.0			
21.0			
22.0			
23.0			
24.0			
25.0			
30.0			
35.0			
40.0			
45.0			
50.0			
55.0			
60.0			
65.0			]]

[[

]]

**Figure 2-61. Lattice 7648 Maximum Local Peaking**

(\* Local peaking based on three void history fractions of 0.0, 0.4 and 0.7)

**Table 2-42. Lattice 7649 Peaking**

Exposure (GWd/ST)	Maximum Local Peaking		
	VF 0.0	VF 0.4	VF 0.7
0.0	[[		
0.2			
1.0			
2.0			
3.0			
4.0			
5.0			
6.0			
7.0			
8.0			
9.0			
10.0			
11.0			
12.0			
13.0			
14.0			
15.0			
16.0			
17.0			
18.0			
19.0			
20.0			
21.0			
22.0			
23.0			
24.0			
25.0			
30.0			
35.0			
40.0			
45.0			
50.0			
55.0			
60.0			
65.0			]]

[[

]]

**Figure 2-62. Lattice 7649 Maximum Local Peaking**

(\* Local peaking based on three void history fractions of 0.0, 0.4 and 0.7)

**Table 2-43. Lattice 7650 Peaking**

Exposure (GWd/ST)	Maximum Local Peaking		
	VF 0.0	VF 0.4	VF 0.7
0.0	[[		
0.2			
1.0			
2.0			
3.0			
4.0			
5.0			
6.0			
7.0			
8.0			
9.0			
10.0			
11.0			
12.0			
13.0			
14.0			
15.0			
16.0			
17.0			
18.0			
19.0			
20.0			
21.0			
22.0			
23.0			
24.0			
25.0			
30.0			
35.0			
40.0			
45.0			
50.0			
55.0			
60.0			
65.0			]]

[[

]]

**Figure 2-63. Lattice 7650 Maximum Local Peaking**

(\* Local peaking based on three void history fractions of 0.0, 0.4 and 0.7)



**Table 2-44. Lattice 7651 Peaking**

Exposure (GWd/ST)	Maximum Local Peaking		
	VF 0.0	VF 0.4	VF 0.7
0.0	[[		
0.2			
1.0			
2.0			
3.0			
4.0			
5.0			
6.0			
7.0			
8.0			
9.0			
10.0			
11.0			
12.0			
13.0			
14.0			
15.0			
16.0			
17.0			
18.0			
19.0			
20.0			
21.0			
22.0			
23.0			
24.0			
25.0			
30.0			
35.0			
40.0			
45.0			
50.0			
55.0			
60.0			
65.0			]]

[[

]]

**Figure 2-64. Lattice 7651 Maximum Local Peaking**

(\* Local peaking based on three void history fractions of 0.0, 0.4 and 0.7)

**Table 2-45. Lattice 7652 Peaking**

Exposure (GWd/ST)	Maximum Local Peaking		
	VF 0.0	VF 0.4	VF 0.7
0.0	[[		
0.2			
1.0			
2.0			
3.0			
4.0			
5.0			
6.0			
7.0			
8.0			
9.0			
10.0			
11.0			
12.0			
13.0			
14.0			
15.0			
16.0			
17.0			
18.0			
19.0			
20.0			
21.0			
22.0			
23.0			
24.0			
25.0			
30.0			
35.0			
40.0			
45.0			
50.0			
55.0			
60.0			
65.0			]]

[[

]]

**Figure 2-65. Lattice 7652 Maximum Local Peaking**

(\* Local peaking based on three void history fractions of 0.0, 0.4 and 0.7)

**Table 2-46. Lattice 7653 Peaking**

Exposure (Gwd/ST)	Maximum Local Peaking		
	VF 0.0	VF 0.4	VF 0.7
0.0	[[		
0.2			
1.0			
2.0			
3.0			
4.0			
5.0			
6.0			
7.0			
8.0			
9.0			
10.0			
11.0			
12.0			
13.0			
14.0			
15.0			
16.0			
17.0			
18.0			
19.0			
20.0			
21.0			
22.0			
23.0			
24.0			
25.0			
30.0			
35.0			
40.0			
45.0			
50.0			
55.0			
60.0			
65.0			]]

[[

]]

**Figure 2-66. Lattice 7653 Maximum Local Peaking**

(\* Local peaking based on three void history fractions of 0.0, 0.4 and 0.7)

Table 2-47. Lattice 7654 Peaking

Exposure (Gwd/ST)	Maximum Local Peaking		
	VF 0.0	VF 0.4	VF 0.7
0.0	[[		
0.2			
1.0			
2.0			
3.0			
4.0			
5.0			
6.0			
7.0			
8.0			
9.0			
10.0			
11.0			
12.0			
13.0			
14.0			
15.0			
16.0			
17.0			
18.0			
19.0			
20.0			
21.0			
22.0			
23.0			
24.0			
25.0			
30.0			
35.0			
40.0			
45.0			
50.0			
55.0			
60.0			
65.0			]]

[[

]]

Figure 2-67. Lattice 7654 Maximum Local Peaking

(\* Local peaking based on three void history fractions of 0.0, 0.4 and 0.7)

**Table 2-48. Lattice 7655 Peaking**

Exposure (GWd/ST)	Maximum Local Peaking		
	VF 0.0	VF 0.4	VF 0.7
0.0	[[		
0.2			
1.0			
2.0			
3.0			
4.0			
5.0			
6.0			
7.0			
8.0			
9.0			
10.0			
11.0			
12.0			
13.0			
14.0			
15.0			
16.0			
17.0			
18.0			
19.0			
20.0			
21.0			
22.0			
23.0			
24.0			
25.0			
30.0			
35.0			
40.0			
45.0			
50.0			
55.0			
60.0			
65.0			]]

[[

]]

**Figure 2-68. Lattice 7655 Maximum Local Peaking**

(\* Local peaking based on three void history fractions of 0.0, 0.4 and 0.7)

[[

]]

**Figure 2-69. Rod Local Peaking (Bundle 2990, Lattice 7633, VF=40%, BOL)**

[[

]]

**Figure 2-70. Rod Local Peaking (Bundle 2991, Lattice 7638, VF=40%, BOL)**

[[

]]

**Figure 2-71. Rod Local Peaking (Bundle 2992, Lattice 7644, VF=40%, BOL)**



[[

]]

**Figure 2-72. Rod Local Peaking (Bundle 2993, Lattice 7648, VF=40%, BOL)**

[[

]]

**Figure 2-73. Rod Local Peaking (Bundle 2994, Lattice 7652, VF=40%, BOL)**

**Table 2-49. Bundle 2990 Uncontrolled and Controlled R-Factors**

<b>Exposure (GWd/ST)</b>	<b>R-Factor (Fully Uncontrolled)</b>	<b>R-Factor (Fully Controlled)</b>
0.0	[[	
0.2		
1.0		
2.0		
3.0		
4.0		
5.0		
6.0		
7.0		
8.0		
9.0		
10.0		
11.0		
12.0		
13.0		
14.0		
15.0		
16.0		
17.0		
18.0		
19.0		
20.0		
21.0		
22.0		
23.0		
24.0		
25.0		
30.0		
35.0		
40.0		
45.0		
50.0		
55.0		
60.0		
65.0		]]

**Table 2-50. Bundle 2991 Uncontrolled and Controlled R-Factors**

<b>Exposure (GWd/ST)</b>	<b>R-Factor (Fully Uncontrolled)</b>	<b>R-Factor (Fully Controlled)</b>
0.0	[[	
0.2		
1.0		
2.0		
3.0		
4.0		
5.0		
6.0		
7.0		
8.0		
9.0		
10.0		
11.0		
12.0		
13.0		
14.0		
15.0		
16.0		
17.0		
18.0		
19.0		
20.0		
21.0		
22.0		
23.0		
24.0		
25.0		
30.0		
35.0		
40.0		
45.0		
50.0		
55.0		
60.0		
65.0		]]

**Table 2-51. Bundle 2992 Uncontrolled and Controlled R-Factors**

<b>Exposure (GWd/ST)</b>	<b>R-Factor (Fully Uncontrolled)</b>	<b>R-Factor (Fully Controlled)</b>
0.0	[[	
0.2		
1.0		
2.0		
3.0		
4.0		
5.0		
6.0		
7.0		
8.0		
9.0		
10.0		
11.0		
12.0		
13.0		
14.0		
15.0		
16.0		
17.0		
18.0		
19.0		
20.0		
21.0		
22.0		
23.0		
24.0		
25.0		
30.0		
35.0		
40.0		
45.0		
50.0		
55.0		
60.0		
65.0		]]

**Table 2-52. Bundle 2993 Uncontrolled and Controlled R-Factors**

<b>Exposure (GWd/ST)</b>	<b>R-Factor (Fully Uncontrolled)</b>	<b>R-Factor (Fully Controlled)</b>
0.0	[[	
0.2		
1.0		
2.0		
3.0		
4.0		
5.0		
6.0		
7.0		
8.0		
9.0		
10.0		
11.0		
12.0		
13.0		
14.0		
15.0		
16.0		
17.0		
18.0		
19.0		
20.0		
21.0		
22.0		
23.0		
24.0		
25.0		
30.0		
35.0		
40.0		
45.0		
50.0		
55.0		
60.0		
65.0		]]

**Table 2-53. Bundle 2994 Uncontrolled and Controlled R-Factors**

<b>Exposure (GWd/ST)</b>	<b>R-Factor (Fully Uncontrolled)</b>	<b>R-Factor (Fully Controlled)</b>
0.0	[[	
0.2		
1.0		
2.0		
3.0		
4.0		
5.0		
6.0		
7.0		
8.0		
9.0		
10.0		
11.0		
12.0		
13.0		
14.0		
15.0		
16.0		
17.0		
18.0		
19.0		
20.0		
21.0		
22.0		
23.0		
24.0		
25.0		
30.0		
35.0		
40.0		
45.0		
50.0		
55.0		
60.0		
65.0		]]

[[

]]

**Figure 2-74. Uncontrolled Rod R-Factors (Bundle 2990, 20 GWD/ST)**



[[

]]

**Figure 2-75. Uncontrolled Rod R-Factors (Bundle 2991, 20 GWD/ST)**

[[

]]

**Figure 2-76. Uncontrolled Rod R-Factors (Bundle 2992, 20 GWD/ST)**

[[

]]

**Figure 2-77. Uncontrolled Rod R-Factors (Bundle 2993, 20 GWD/ST)**

[[

]]

**Figure 2-78. Uncontrolled Rod R-Factors (Bundle 2994, 20 GWD/ST)**

Table 2-54. Lattice 7633 K-∞

Exposure (GWd/ST)	K-infinity (40% VF)	
	HOTUNC	HOTUNC D
0.0	[[	
0.2		
1.0		
2.0		
3.0		
4.0		
5.0		
6.0		
7.0		
8.0		
9.0		
10.0		
11.0		
12.0		
13.0		
14.0		
15.0		
16.0		
17.0		
18.0		
19.0		
20.0		
21.0		
22.0		
23.0		
24.0		
25.0		
30.0		
35.0		
40.0		
45.0		
50.0		
55.0		
60.0		
65.0		]]

[[

]]

Figure 2-79. Bundle 2990 Lattice 7633 K-infinity at 40% VF

Table 2-55. Lattice 7638 K-∞

Exposure (GWd/ST)	K-infinity (40% VF)	
	HOTUNC	HOTUNC D
0.0	[[	
0.2		
1.0		
2.0		
3.0		
4.0		
5.0		
6.0		
7.0		
8.0		
9.0		
10.0		
11.0		
12.0		
13.0		
14.0		
15.0		
16.0		
17.0		
18.0		
19.0		
20.0		
21.0		
22.0		
23.0		
24.0		
25.0		
30.0		
35.0		
40.0		
45.0		
50.0		
55.0		
60.0		
65.0		]]

[[

]]

Figure 2-80. Bundle 2991 Lattice 7638 K-infinity at 40% VF

Table 2-56. Lattice 7644 K-∞

Exposure (GWd/ST)	K-infinity (40% VF)	
	HOTUNC	HOTUNCD
0.0	[[	
0.2		
1.0		
2.0		
3.0		
4.0		
5.0		
6.0		
7.0		
8.0		
9.0		
10.0		
11.0		
12.0		
13.0		
14.0		
15.0		
16.0		
17.0		
18.0		
19.0		
20.0		
21.0		
22.0		
23.0		
24.0		
25.0		
30.0		
35.0		
40.0		
45.0		
50.0		
55.0		
60.0		
65.0		]]

[[

]]

Figure 2-81. Bundle 2992 Lattice 7644 K-infinity at 40% VF

Table 2-57. Lattice 7648 K-∞

Exposure (GWd/ST)	K-infinity (40% VF)	
	HOTUNC	HOTUNC D
0.0	[[	
0.2		
1.0		
2.0		
3.0		
4.0		
5.0		
6.0		
7.0		
8.0		
9.0		
10.0		
11.0		
12.0		
13.0		
14.0		
15.0		
16.0		
17.0		
18.0		
19.0		
20.0		
21.0		
22.0		
23.0		
24.0		
25.0		
30.0		
35.0		
40.0		
45.0		
50.0		
55.0		
60.0		
65.0		]]

[[

]]

Figure 2-82. Bundle 2993 Lattice 7648 K-infinity at 40% VF



Table 2-58. Lattice 7652 K-∞

Exposure (GWd/ST)	K-infinity (40% VF)	
	HOTUNC	HOTUNCD
0.0	[[	
0.2		
1.0		
2.0		
3.0		
4.0		
5.0		
6.0		
7.0		
8.0		
9.0		
10.0		
11.0		
12.0		
13.0		
14.0		
15.0		
16.0	/	
17.0		
18.0		
19.0		
20.0		
21.0		
22.0		
23.0		
24.0		
25.0		
30.0		
35.0		
40.0		
45.0		
50.0		
55.0		
60.0		
65.0		]]

[[

]]

Figure 2-83. Bundle 2994 Lattice 7652 K-infinity at 40% VF

### 3. CORE NUCLEAR DESIGN EVALUATION

The ESBWR core design is performed using the same analytical tools and methods that are applied to steady-state nuclear evaluations of all General Electric BWR cores. These nuclear physics methods, which are described in Reference 1, have proven their abilities and capabilities over hundreds of reactor operating years. This section describes the various core analyses and results for the ESBWR reference initial core based on these methods.

#### 3.1 Nuclear Design and Core Loading Pattern Description

The ESBWR is rated at 4500 MWth and consists of 1132 bundles and 269 control blades. The three-dimensional simulation modeling of the reference initial core design was performed assuming quarter core mirror symmetry. Consequently, results in the upper left quadrant will be mirrored in the remaining three quadrants. Below are the nominal operating conditions for the ESBWR reference initial core.

Parameter	Nominal Value
Power (MWth)	4500
Flow (Mlb/hr)	[[
Dome Pressure (psia)	
Bypass (%)	
Core Inlet Temperature (°F)	]]

The reference initial core design is characterized by the fuel type loading pattern given in Figure 3-1. The reference design incorporates the unique GE14E bundle designs previously described in Section 2 to achieve optimum core performance (i.e., thermal limits, hot excess reactivity, cold shutdown margin, etc.) for an initial cycle utilizing the Control Cell Core (CCC) loading strategy. As previously discussed, the lattice enrichments and gadolinia concentrations have been carefully selected to achieve the desired k-infinity and local peaking behavior and the lattice arrangements, or zones, within each bundle have been chosen to yield the desired axial power characteristics when assembled in the core. The bundle types and quantities are also shown in Figure 3-1. The lowest enrichment assembly, shown as IAT number 4, is placed in peripheral core locations where neutron leakage is highest. [[

]] For a traditional CCC loading strategy, the A-2 control rod locations typically contain the next lowest reactivity bundles, with the lowest reactivity bundles reserved for peripheral locations. The CCC core design limits control rod movement to a fixed group of control rods and control rod motion occurs adjacent only to low power fuel. This strategy results in reduced control blade history effects and simplified operation. [[

]] These assemblies are located in the central region of the core, with the higher of the two

enrichments placed toward the outer region. This selection helps to achieve a relatively flatter radial power profile and improved thermal margins. The remaining core locations are between this medium enriched central region and the periphery. [[

]] Placement of the highest enrichment assemblies in this region of the core also contributes to an improved radial power profile. The overall core average enrichment of this initial core design is [[

This reference core is designed [[

]].

### 3.2 Eigenvalue Determination

At the beginning of a core design effort, hot and cold eigenvalues are determined in order to calibrate the 3D simulator predictions to actual results of the BWR fleet. Because of the similarities between current operating BWRs and the ESBWR, as well as the identical nature of the lattice physics calculations, exposure dependent eigenvalues could be obtained. Incorporating the actual trends of other large BWR cores, the hot and cold exposure dependent eigenvalues were determined. Table 3-1 and Figure 3-2 show the design basis exposure dependent hot eigenvalue. Table 3-2 and Figure 3-3 show the design basis exposure dependent cold eigenvalue. Eigenvalue determination is used for hot and cold reactivity calculations as well as determining the appropriate control rod inventory needed to provide criticality at full power conditions.

### 3.3 Control Rod Patterns Including Axial Power Considerations

Figure 3-4 illustrates the control rod patterns for this reference initial core. The maximum number of control rod notches per control blade is defined as 80. That is, for this simulation, a control rod at notch 80 is fully withdrawn; a control rod at notch 0 is fully inserted. The rod patterns utilize [[

]], maximizes operating capacity factor, and provides for improved fuel cycle efficiency.

An inherent advantage of the ESBWR is the improved fuel cycle efficiency due to spectral shift that is a function of axial power shape control. By achieving a bottom peaked core average axial power shape, the presence of voids in the middle and top of the core provides an environment helpful in creating additional fuel in the form of plutonium. Consequently, additional full power capability is provided towards EOC as the axial shape slowly migrates towards the top and the plutonium is utilized. This classic BWR characteristic is well illustrated in Figures 3-5 through 3-8, which illustrates the progression in axial power shape throughout each of the major control rod sequences from BOC to EOC. Core average axial power results are also provided in Tables 3-3 through 3-6. Figures 3-9 through 3-12 illustrate the core average axial exposure shape from BOC to EOC for each control rod sequence. Corresponding exposure results are provided in Tables 3-7 through 3-10.

With regard to the target rod patterns, it was previously mentioned that the control rods are selected based on the design basis hot critical eigenvalue as well as thermal limit considerations. Table 3-11 and Figure 3-13 illustrate how well the target control rod patterns satisfy the design basis hot critical eigenvalue. The 2-D EOC bundle average exposure distribution at the end of this rodged burn scenario is shown in Figure 3-14.

### 3.4 Integrated Power Distribution

Although a bundle integrated power constraint does not exist, this is a helpful parameter when understanding loading pattern influence on individual power generation per bundle. During typical BWR non-initial core operation, the once-burnt high reactivity fuel provides the most influence on power distribution. Similarly, towards the EOC the fresh fuel provides most of the influence. In an exposed core, it is this balance of fresh and once burnt fuel that contributes to a more uniform core power distribution. During initial core operation for the ESBWR, however, the desired reactivity and local peaking characteristics are achieved through proper distribution of enrichment and gadolinia within each bundle design as previously discussed in Section 2. The maximum bundle integrated power value, also referred to as radial peaking factor, is shown in Table 3-12 and in Figure 3-15. The maximum range of values in all of these figures [[

]] which are bounded by current operating BWRs. The corresponding 2-D bundle integrated powers at the beginning and end of each main control rod pattern sequence are presented in Figures 3-16 through 3-23.

### 3.5 Thermal Limit Evaluation

The core power distribution is a function of fuel bundle design, core loading, control rod pattern, core exposure distributions and core coolant flow rate. The thermal performance parameters, MLHGR and MCPR, limit the core power distribution. The analysis of the performance of the reference initial core design in terms of power distribution, and the associated MLHGR and MCPR distributions within the core throughout the cycle, are discussed below.

#### 3.5.1 MLHGR

The Maximum Fraction of Linear Power Density (MFLPD) is shown as a function of cycle exposure in Table 3-13 and Figure 3-24. Note that the value plotted in Figure 3-24 represents the maximum value for any node in the core at the specified exposure point. The MFLPD parameter, in general terms, is defined as:

$$\text{MFLPD} = \text{LHGR} / \text{LHGR Limit}$$

It should be noted that the thermal mechanical LHGR limit is exposure dependent, which necessitates establishing the MFLPD parameter to capture this. A MFLPD that is equal to 1.0 corresponds to a rod within a six inch node that is operating at its LHGR limit and any further increases in LHGR result in entering a Technical Specification Limiting Condition of Operation (LCO). Every rod within the node has a MFLPD. The rod with the highest MFLPD in any given node defines the maximum MFLPD and this becomes the nodal MFLPD. The node with the highest MFLPD in an assembly can be thought of as the limiting MFLPD for that assembly. The highest MFLPD for any node in the core corresponds to the most limiting node and defines the minimum operating margin ( $1.0 - \text{MFLPD}$ ) in the reactor core. Figures 3-25 through 3-32 show the 2-D MFLPD distribution at the beginning and end of each main control rod sequence. The MLHGR limit used in the calculation of the MFLPD is reported in Reference 3.

### 3.5.2 MCPR

Table 3-14 and Figure 3-33 illustrate the minimum critical power ratio (MCPR) as a function of exposure throughout the cycle. Figure 3-34 through Figure 3-41 provide the 2-D MCPR distribution at the beginning and end of each control rod sequence. The Operating Limit Minimum Critical Power Ratio (OLMCPR) is expected to be [[ ]]. Therefore, the reference initial core will conform to this OLMCPR with sufficient margin. The initial core OLMCPR is determined in a manner consistent with the equilibrium ESBWR core that was described in Reference 4.

### 3.6 Hot Excess Evaluation

A hot excess reactivity calculation illustrates the amount of excess reactivity a core design provides throughout the cycle. This calculation is performed by withdrawing all control rods at selected state points through the cycle and comparing the difference between the resulting eigenvalue and the design basis hot critical eigenvalue previously shown in Figure 3-2. Table 3-15 and Figure 3-42 shows the hot excess reactivity for this reference initial core design. The BOC hot excess is estimated to be [[ ]]

]] However, control rod sequence adjustments are still adopted to moderate the effects of CBH and to improve exposure burn-up and fuel cycle efficiency.

The excess reactivity described above is designed into the core and controlled by the control rod system and supplemented by gadolinia-urania fuel rods discussed in Section 2. Gadolinia is used to provide partial control of the excess reactivity available during the fuel cycle. The burnable absorber loading controls local peaking behavior and suppresses the reactivity of the fuel bundle. An optimum bundle design will utilize a sufficient number of gadolinia rods to suppress core reactivity at BOC and a sufficient concentration to limit the peak reactivity to a manageable level throughout the cycle with little remaining residual gadolinia at EOC. The burnable absorber reduces the requirement for control rod inventory. Control rods are used primarily to compensate for reactivity changes due to burn-up and to maintain an acceptable core power

distribution. A detailed description of the ESBWR initial core bundle designs was presented in Section 2.

### 3.7 Cold Shutdown Margin Evaluation

The ESBWR control rod system is designed to provide adequate shutdown margin and control of the maximum excess reactivity anticipated during plant operation. For this evaluation the core is assumed to be in the cold, xenon-free condition in order to ensure that the calculated values are conservative. Further discussion of the uncertainty of these calculations is given in Reference 5.

Shutdown margin results through the cycle are shown in Table 3-16 and in Figure 3-44. The shutdown margin is evaluated by calculating the core neutron multiplication with the core simulator at selected exposure points, assuming the highest worth control rod, or rod pair, is stuck in the fully withdrawn position. Since two control rod drives are assigned to a single Hydraulic Control Unit (HCU) for the ESBWR, the shutdown margin evaluation assumes that a rod pair is stuck in the fully withdrawn position. The control rod drive to HCU assignments are shown in Figure 3-43. Note that since there is an odd number of control rods, there is one HCU that is assigned a single control rod; this is HCU number 51, which is in the very center of the core. Since all rod pairs were selected with sufficient separation between them, they may be considered loosely coupled. Figures 3-45 to 3-47 are provided to demonstrate this loose coupling. Control rod worths at BOC, MOC and EOC are compared for the HCU rod pair withdrawn and the corresponding strongest single rod of the rod pair withdrawn. Control rod worths are shown to be essentially the same for the forty highest worth HCUs in the top half of the core. Given that the core loading is quadrant symmetric, and HCU assignments are half core rotational symmetric, comparing the worths for the forty highest worth HCUs effectively covers about 60% of the total control rods in the ESBWR. Consequently, 2-D SDM results and SDM results through the cycle based on the highest worth single rod out can be considered equivalent to SDM results for the strongest HCU rod pair withdrawn. A cycle specific assessment shall be performed every cycle to validate this conclusion.

The cold k-eff is calculated with the highest worth control rod, or rod pair, out at various exposures through the cycle. A value R is defined as the difference between the highest worth rod pair out k-eff at beginning of cycle (BOC) and the maximum calculated highest worth rod pair out k-eff at any exposure point. For the ESBWR reference initial core, the minimum shutdown margin occurs at BOC; thus, the value of R is zero. The calculated k-eff values with all control rods fully inserted ( $k_{CARI}$ ) and with the strongest rod fully out ( $k_{SRO}$ ) are shown below at BOC, MOC (defined as 5.0 GWd/ST) and EOC conditions. Also shown is the corresponding cold critical design bases eigenvalue ( $k_{CRIT}$ ).

Control Configuration	BOC K-eff	MOC K-eff	EOC K-eff
Fully Controlled ( $k_{CARI}$ )	[[		
Strongest Rod Out ( $k_{SRO}$ )			
Critical k-effective ( $k_{CRIT}$ )			]]

Based on the design  $k_{CRIT}$  value, the predicted shutdown margin is [[  
]], which is significantly above the minimum required technical specification shutdown margin

value. Additional 2-D SDM results are provided in Figures 3-48 through 3-50 at BOC, MOC and EOC conditions. Note that these figures report the SDM for a single control rod withdrawn in the upper left quadrant. For a HCU rod pair, the SDM would be equal to the lowest value of the two control rods that are assigned to the HCU.

### **3.8 Standby Liquid Control System Evaluation**

The Standby Liquid Control System (SLCS) is designed to provide the capability of bringing the reactor, at any time in a cycle, from full power with a minimum control rod inventory (which is defined to be at the peak of the xenon transient) to a sub-critical condition with the reactor in the most reactive xenon-free state.

The requirements of this system are dependent primarily on the reactor power level and on the reactivity effects of voids and temperature between full power and cold, xenon-free conditions. The shutdown margin is calculated for a uniformly mixed equivalent concentration of natural boron, which is required in the reactor core to provide adequate cold shutdown margin after initiation of the SLCS. Calculations are performed throughout the cycle including the most reactive critical, xenon-free condition. Calculations are performed with all control rods withdrawn. The shutdown capability of the SLCS for the ESBWR reference initial core was calculated using [[

]]. Table 3-17 and Figure 3-51 shows that significant SLCS shutdown margin exists for the ESBWR core compared to a limit of 1%.

### **3.9 Criticality of Reactor During Refueling Evaluation**

The basis for maintaining the reactor in a sub-critical condition during refueling is presented in Subsection 1.2, and a discussion of how control requirements are met is given in Section 3.7. The minimum required shutdown margin is given in the technical specifications.

### **3.10 Negative Reactivity Feedback Evaluation**

Reactivity coefficients are a measure of the differential changes in reactivity produced by differential changes in core conditions. These coefficients are useful in understanding the response of the core to external disturbances. The Doppler reactivity coefficient, previously discussed in Section 2, and the moderator void reactivity coefficient are the two primary reactivity coefficients that characterize the dynamic behavior of BWRs.

The safety analysis methods are based on system and core models that include an explicit representation of the core space-time kinetics. Therefore, the reactivity coefficients are not directly used in the safety analysis methods, but are useful in the general understanding and discussion of the core response to perturbations.

#### **3.10.1 Moderator Temperature Coefficient Evaluation**

The moderator temperature coefficient (MTC) is associated with the change in the water moderating capability. A negative MTC during power operation provides inherent protection against power excursions. Hot standby is the condition under which the BWR core coolant has reached rated pressure and the temperature at which boiling has begun. Once boiling begins, the moderator temperature remains essentially constant in the boiling regions.

Analyses of the MTC of the reference initial core design were performed. Table 3-18 and Figure 3-52 show the eigenvalues as a function of moderator temperature at three exposure state points for the critical rod pattern configuration determined with xenon. This conservative analysis condition might be expected to occur during a plant startup that immediately follows plant shutdown (e.g., reactor scram). The accumulation of xenon would result in a lower critical control fraction that results in a less negative MTC. These eigenvalues were then used to determine the MTC for the reference initial core. The variation of the MTC as a function of temperature is shown in Table 3-19 and Figure 3-53 for three exposure points through the cycle.

The most limiting state condition was determined to be at the end of the reference initial cycle for the critical core configuration. The results demonstrated that the MTC is [[

]]

The results of these analyses at these conditions indicate that the moderator temperature coefficient is negative for all moderator temperatures in the operating temperature range.

### 3.10.2 Moderator Void Coefficient Evaluation

The moderator void coefficient (MVC) should be large enough to prevent power oscillation due to spatial xenon changes yet small enough that pressurization transients do not unduly limit plant operation. In addition, the MVC has the ability to flatten the radial power distribution and to provide ease of reactor control due to the void feedback mechanism. The overall MVC is always negative over the complete operating range.

Analyses of the MVC of the reference initial core design show that boiling of the moderator in the active channel flow area results in negative reactivity feedback for all expected modes of operation. The operating mode selected to represent the most limiting condition (the least negative value of moderator void coefficient) was the cold critical state at the end of the initial cycle. Table 3-20 and Figure 3-54 show the variation in eigenvalue as a function of moderator temperature and voids at three exposure state points for the critical rod configuration determined with xenon. These eigenvalues were then used to determine the MVC for the reference initial core. The variation of the MVC as a function of temperature is shown in Table 3-21 and Figure 3-55 for three exposure points through the cycle.

### 3.11 Xenon Stability Evaluation

Boiling water reactors do not have instability problems due to xenon. This has been demonstrated by:

- Never having observed xenon instabilities in operating BWRs;
- Special tests which have been conducted on operating BWRs in an attempt to force the reactor into xenon instability; and
- Calculations.

All of these indicators have proven that xenon transients are highly damped in a BWR due to the large negative moderator void feedback. Xenon stability analysis and experiments are reported in Reference 6. Specific evaluations demonstrating the damping of xenon transients (oscillations) for the ESBWR equilibrium core are reported in Reference 1.



### 3.11.1 BWR Xenon Trends

Spatial stability measurements and analytical studies for the current BWR fleet have demonstrated very stable xenon transient performance characteristics. This stability is attributed to the large negative power coefficient that characterizes the BWR design. The negative power coefficient provides for strong spatial damping of transient reactor performance that results from xenon transients. The ESBWR shares the same negative power coefficient characteristics with current BWR designs, and is similarly stable with respect to xenon transient performance.

The large negative power coefficient of reactivity is a unique characteristic that results from moderator boiling. The large change in moderator density in the boiling environment of the reactor core is primarily responsible for the large negative power coefficient.

Non-linear trends also exist in the axial xenon distributions in an ESBWR core. As the moderator density changes axially in the reactor core, the neutron spectrum also changes. As the moderator density decreases, the neutron spectrum hardens. Since the  $\text{Xe}^{135}$  isotope has a smaller absorption cross section at higher neutron energies, the  $\text{Xe}^{135}$  distribution is affected axially by the non-uniform moderator density. The  $\text{I}^{135}$  isotope, which decays to produce  $\text{Xe}^{135}$ , is substantially proportional to the axial power distribution as it is a direct result of the fission process, and is not strongly affected by the axial changes in the neutron spectrum. The resulting differences in the  $\text{Xe}^{135}$  and  $\text{I}^{135}$  distributions lead to non-linear axial trends in the transient performance, which help to dampen any oscillatory behavior caused by transient concentration differences.

The non-linear axial trends in nuclear characteristics, coupled with the negative power coefficient resulting from the non-uniform moderator density, result in non-linear axial responses that cause axial xenon redistributions to be damped in one cycle. Additionally, although large reactor cores exhibit loosely coupled characteristics, local feedback at each point in the reactor core is provided by moderator boiling. The large negative power coefficient, coupled with the local feedback provided by localized boiling, work together to effectively damp azimuthal and radial oscillations.

The physical and nuclear characteristics of the ESBWR design have different effects upon the magnitude of the power coefficient. A summary of the important design characteristics and their influence on the power coefficient are shown below. These characteristics are consistent between BWR and ESBWR designs.

Increased Variable	Effect on Power Coefficient
moderator to fuel ratio	less negative
fuel rod diameter	less negative
fuel enrichment	more negative
fuel exposure	less negative
bypass water fraction	less negative
core size	less negative
void content	more negative

The primary differences between current operating BWRs and the ESBWR design include core size, core height, and the lack of forced recirculation flow in the ESBWR. The ESBWR core design is larger than the largest operating BWR (1132 bundles vs. 872 bundles). However the active fuel height for the ESBWR is 20% shorter than current BWR fuel designs. This results in slightly improved xenon stability for the ESBWR since the axial moderator density change associated with boiling occurs over a shorter distance. The natural recirculation characteristic of the ESBWR is also an important difference, because most power maneuvers require the use of control rods to control core reactivity and core power. The control rods have a strong negative influence on the power coefficient. Control rod worth increases rapidly as water density is decreased because of the increase in the thermal neutron diffusion length with decreased moderator density. The required use of control rods to control core power complements the negative power coefficient associated with the non-uniform moderator density to effectively damp transient xenon effects.

### **3.11.2 ESBWR Xenon Transient Conclusions**

The negative power coefficient trends of an ESBWR have a pronounced effect on spatial xenon stability. The negative power coefficient results naturally from the non-uniform moderator distribution in the reactor core. This characteristic, coupled with the non-linear axial trends in nuclear characteristics, result in non-linear axial responses that cause the effects of xenon transients to be damped in one cycle. The effects of localized boiling provide direct local feedback that suppresses radial and azimuthal perturbations.

### **3.12 Summary**

This section presented key core performance characteristics of the ESBWR reference initial core loading the GE14E fuel design. For the reference core loading pattern, a detailed rodged depletion evaluation was performed using PANACEA. The evaluation confirmed that thermal margins (i.e., MCPR and MFLPD) and reactivity margins (i.e., hot excess and cold shutdown) could be achieved. In addition, all nuclear design requirements as defined in Section 1 were satisfied.

[[

]]

**Figure 3-1. Reference Initial Core Fuel Types and Quantities**

**Table 3-1. Hot Design Eigenvalues**

Exposure (MWd/ST)	Hot Design K-eff
[[	
	]]

[[

]]

**Figure 3-2. Hot Design Eigenvalue vs. Exposure**

Table 3-2. Cold Design Eigenvalues

Exposure (MWd/ST)	Distributed K-eff	Local K-eff
[[		
		]]

[[ ]]

Figure 3-3. Cold Design Eigenvalue vs. Exposure

[[

]]

**Figure 3-4. Rod Patterns**

[[

**Figure 3-4. Rod Patterns (Continued)**

]]

[[

**Figure 3-4. Rod Patterns (Continued)**

]]



[[

**Figure 3-4. Rod Patterns (Continued)**

]]

[[

**Figure 3-4. Rod Patterns (Continued)**

]]

[[

**Figure 3-4. Rod Patterns (Continued)**

]]

[[

**Figure 3-4. Rod Patterns (Continued)**

]]

[[

**Figure 3-4. Rod Patterns (Continued)**

]]

**Table 3-3. Axial Nodal Power Seq-1**

<b>Axial Node</b>	<b>Beginning of Sequence 1 Axial Power</b>	<b>End of Sequence 1 Axial Power</b>
20	[[	
19		
18		
17		
16		
15		
14		
13		
12		
11		
10		
9		
8		
7		
6		
5		
4		
3		
2		
1		]]

[[

]]

**Figure 3-5. Sequence 1 Core Average Axial Power Distributions**

Table 3-4. Axial Nodal Power Seq-2

Axial Node	Beginning of Sequence 2 Axial Power	End of Sequence 2 Axial Power
20	[[	
19		
18		
17		
16		
15		
14		
13		
12		
11		
10		
9		
8		
7		
6		
5		
4		
3		
2		
1		]]

[[

]]

Figure 3-6. Sequence 2 Core Average Axial Power Distributions

Table 3-5. Axial Nodal Power Seq-3

Axial Node	Beginning of Sequence 3 Axial Power	End of Sequence 3 Axial Power
20	[[	
19		
18		
17		
16		
15		
14		
13		
12		
11		
10		
9		
8		
7		
6		
5		
4		
3		
2		
1		]]

[[ ]]

Figure 3-7. Sequence 3 Core Average Axial Power Distributions



**Table 3-6. Axial Nodal Power Seq-4**

<b>Axial Node</b>	<b>Beginning of Sequence 4 Axial Power</b>	<b>End of Sequence 4 Axial Power</b>
20	[[	
19		
18		
17		
16		
15		
14		
13		
12		
11		
10		
9		
8		
7		
6		
5		
4		
3		
2		
1		]]

[[ ]]

**Figure 3-8. Sequence 4 Core Average Axial Power Distributions**

Table 3-7. Axial Nodal Exposure Seq-1

Axial Node	Beginning of Sequence 1 Axial Exposure	End of Sequence 1 Axial Exposure
20	[[	
19		
18		
17		
16		
15		
14		
13		
12		
11		
10		
9		
8		
7		
6		
5		
4		
3		
2		
1		]]

[[ ]]

Figure 3-9. Sequence 1 Core Average Axial Exposure Distributions

**Table 3-8. Axial Nodal Exposure Seq-2**

<b>Axial Node</b>	<b>Beginning of Sequence 2 Axial Exposure</b>	<b>End of Sequence 2 Axial Exposure</b>
20	[[	
19		
18		
17		
16		
15		
14		
13		
12		
11		
10		
9		
8		
7		
6		
5		
4		
3		
2		
1		]]

[[ ]]

**Figure 3-10. Sequence 2 Core Average Axial Exposure Distributions**

**Table 3-9. Axial Nodal Exposure Seq-3**

<b>Axial Node</b>	<b>Beginning of Sequence 3 Axial Exposure</b>	<b>End of Sequence 3 Axial Exposure</b>
<b>20</b>	[[	
<b>19</b>		
<b>18</b>		
<b>17</b>		
<b>16</b>		
<b>15</b>		
<b>14</b>		
<b>13</b>		
<b>12</b>		
<b>11</b>		
<b>10</b>		
<b>9</b>		
<b>8</b>		
<b>7</b>		
<b>6</b>		
<b>5</b>		
<b>4</b>		
<b>3</b>		
<b>2</b>		
<b>1</b>		]]

[[ ]]

**Figure 3-11. Sequence 3 Core Average Axial Exposure Distributions**

Table 3-10. Axial Nodal Exposure Seq-4

Axial Node	Beginning of Sequence 4 Axial Exposure	End of Sequence 4 Axial Exposure
20	[[	
19		
18		
17		
16		
15		
14		
13		
12		
11		
10		
9		
8		
7		
6		
5		
4		
3		
2		
1		]]

[[ ]]

Figure 3-12. Sequence 4 Core Average Axial Exposure Distributions

**Table 3-11. Hot K-eff vs Exposure**

[illegible]

**Figure 3-13. Hot Eigenvalue vs. Cycle Exposure**

[[

]]

**Figure 3-14. End of Cycle Bundle Average Exposure (10.98 GWd/ST)**

### Table 3-12. RPF vs Exposure

[illegible]

**Figure 3-15. Radial Peaking Factor vs. Cycle Exposure**



[[

]]

**Figure 3-16. Beginning of Sequence 1 Integrated Bundle Power (0.0 GWd/ST)**

[[

]]

**Figure 3-17. End of Sequence 1 Integrated Bundle Power (2.5 GWd/ST)**

[[

]]

**Figure 3-18. Beginning of Sequence 2 Integrated Bundle Power (2.5 GWd/ST)**

[[

]]

**Figure 3-19. End of Sequence 2 Integrated Bundle Power (5.0 GWd/ST)**

[[

]]

**Figure 3-20. Beginning of Sequence 3 Integrated Bundle Power (5.0 GWd/ST)**

[[

]]

**Figure 3-21. End of Sequence 3 Integrated Bundle Power (7.5 MWd/ST)**

[[

]]

**Figure 3-22. Beginning of Sequence 4 Integrated Bundle Power (7.5 MWd/ST)**

[[

]]

**Figure 3-23. End of Sequence 4 Integrated Bundle Power (10.98 GWd/ST)**



**Table 3-13. MFLPD vs Exposure**

[illegible]

**Figure 3-24. MFLPD vs. Cycle Exposure**

[[

]]

**Figure 3-25. Beginning of Sequence 1 MFLPD (0.0 GWd/ST)**

[[

]]

**Figure 3-26. End of Sequence 1 MFLPD (2.5 GWd/ST)**

[[

]]

**Figure 3-27. Beginning of Sequence 2 MFLPD (2.5 GWd/ST)**

[[

]]

**Figure 3-28. End of Sequence 2 MFLPD (5.0 GWd/ST)**

[[

]]

**Figure 3-29. Beginning of Sequence 3 MFLPD (5.0 GWd/ST)**

[[

]]

**Figure 3-30. End of Sequence 3 MFLPD (7.5 MWd/ST)**

[[

]]

**Figure 3-31. Beginning of Sequence 4 MFLPD (7.5 MWd/ST)**



[[

]]

**Figure 3-32. End of Sequence 4 MFLPD (10.98 GWd/ST)**

**Table 3-14. MCPR vs Exposure**

[illegible]

**Figure 3-33. MCPR vs. Cycle Exposure**

[[

]]

**Figure 3-34. Beginning of Sequence 1 MCPR (0.0 GWd/ST)**

[[

]]

**Figure 3-35. End of Sequence 1 MCPR (2.5 GWd/ST)**

[[

]]

**Figure 3-36. Beginning of Sequence 2 MCPR (2.5 GWd/ST)**

[[

]]

**Figure 3-37. End of Sequence 2 MCPR (5.0 GWd/ST)**

[[

]]

**Figure 3-38. Beginning of Sequence 3 MCPR (5.0 GWd/ST)**

[[

]]

**Figure 3-39. End of Sequence 3 MCPR (7.5 MWd/ST)**



[[

]]

**Figure 3-40. Beginning of Sequence 4 MCPR (7.5 GWd/ST)**

[[

]]

**Figure 3-41. End of Sequence 4 MCPR (10.98 GWd/ST)**

Table 3-15. Hot Excess Reactivity

Exposure (MWD/ST)	Hot Excess (%)
[[	
	]]

[[ ]]

Figure 3-42. Hot Excess Reactivity vs. Cycle Exposure

[[

]]

**Figure 3-43. Hydraulic Control Unit Assignments**

Table 3-16. Cold Shutdown Margin

Exposure (MWD/ST)	Cold SDM (%)
[[	
	]]

[[

]]

Figure 3-44. Cold Shutdown Margin vs. Cycle Exposure

[[

]]

**Figure 3-45. Control Rod Worth Comparisons at BOC (0.00 GWd/ST)**

[[

]]

**Figure 3-46. Control Rod Worth Comparisons at MOC (5.00 GWd/ST)**

[[

]]

**Figure 3-47. Control Rod Worth Comparisons at EOC (10.98 GWd/ST)**



[[ ]]

**Figure 3-48. Cold Shutdown Margin Distribution (%) at BOC (0.0 GWd/ST)**

[[

]]

**Figure 3-49. Cold Shutdown Margin Distribution (%) at MOC (5.0 GWd/ST)**

[[

]]

**Figure 3-50. Cold Shutdown Margin Distribution (%) at EOC (10.98 GWd/ST)**

Table 3-17. SLCS Shutdown Margin

Exposure (MWD/ST)	SLCS (%)
[[	
	]]

[[

]]

Figure 3-51. Standby Liquid Control Margin vs. Cycle Exposure

Table 3-18. Eigenvalues for MTC/Xenon

Temperature (°C)	Eigenvalue
BOC	
[[	
	]]
MOC	
[[	
	]]
EOC	
[[	
	]]

[[ ]]

Figure 3-52. Eigenvalues vs. Moderator Temperature (for MTC/Xenon)

Table 3-19. MTC with Xenon

Temperature (°C)	MTC (1/k)(dk/dT)
BOC	
[[	
	]]
MOC	
[[	
	]]
EOC	
[[	
	]]

[[ ]]

Figure 3-53. Moderator Temperature Coefficient with Xenon

Table 3-20. Eigenvalues for MVC/Xenon

Temperature (°C)	Eigenvalue 0% Void	Eigenvalue 5% Void
BOC		
[[		
		]]
MOC		
[[		
		]]
EOC		
[[		
		]]

[[ ]]

Figure 3-54. Eigenvalues vs. Moderator Temperature (for MVC/Xenon)

Table 3-21. MVC with Xenon

Temperature (°C)	MVC (1/k)(dk/dV)
BOC	
[[	
	]]
MOC	
[[	
	]]
EOC	
[[	
	]]

[[ ]]

Figure 3-55. Moderator Void Coefficient with Xenon



#### **4. REFERENCES**

1. General Electric Company, "GE14 for ESBWR Nuclear Design Report," NEDC-33239P, Rev. 4, March 2009.
2. Global Nuclear Fuel, "GE14 Compliance With Amendment 22 of NEDE-24011-P-A (GESTAR II)," NEDC-32868P, Rev. 2, September 2007.
3. General Electric Company, "GE14 for ESBWR Fuel Rod Thermal-Mechanical Design Report," NEDC-33242P, Rev. 1, February 2007.
4. General Electric Company, "GE14 for ESBWR – Critical Power Correlation, Uncertainty, and OLMCPR Development," NEDC-33237P, Rev. 4, July 2008.
5. General Electric Company, "BWR/4,5,6 Standard Safety Analysis Report," Rev. 2, Chapter 4, June 1977.
6. R.L. Crowther, "Xenon Considerations in Design of Large Boiling Water Reactors," APED-5640, June 1968.

**NEDO-33326-A Revision 1**  
**Attachment 1**

**NRC SAFETY EVALUATION**

**GE14E FOR ESBWR INITIAL CORE NUCLEAR DESIGN  
REPORT**



OFFICIAL USE ONLY – ENCLOSURE 2 CONTAINS PROPRIETARY INFORMATION

UNITED STATES  
NUCLEAR REGULATORY COMMISSION  
WASHINGTON, D.C. 20555-0001

Rec.  
9-13-10

September 7, 2010

10-255

Mr. Jerald G. Head  
Senior Vice President, Regulatory Affairs  
GE Hitachi Nuclear Energy  
3901 Castle Hayne Road MC A-18  
Wilmington, NC 28401

SUBJECT: FINAL SAFETY EVALUATION REVISION 1 FOR GE HITACHI NUCLEAR  
ENERGY LICENSING TOPICAL REPORT NEDC-33326P REVISION 1, "GE14E  
FOR THE ECONOMIC SIMPLIFIED BOILING WATER REACTOR INITIAL  
CORE NUCLEAR DESIGN REPORT"

Dear Mr. Head:

On August 24, 2005, GE Hitachi (GEH) Nuclear Energy submitted the Economic Simplified Boiling Water Reactor (ESBWR) design certification application to the staff of the U.S. Nuclear Regulatory Commission. Subsequently, in support of the design certification, GEH submitted the license topical report (LTR) NEDC-33326P Revision 1, "GE14E for ESBWR Initial Core Nuclear Design Report." The staff has now completed its review of NEDC-33326P Revision 1.

The staff finds NEDC-33326P Revision 1, acceptable for referencing for the ESBWR design certification to the extent specified and under the limitations delineated in the LTRs and in the associated safety evaluation (SE). The SE, which is enclosed, defines the basis for acceptance of the LTR.

The staff requests that GEH publish the revised version of the LTRs listed above within 1 month of receipt of this letter. The accepted version of NEDC-33326P shall incorporate this letter and the enclosed SE and add an "-A" (designated accepted) following the report identification number.

If NRC's criteria or regulations change, so that its conclusion that the LTR is acceptable is invalidated, GEH and/or the applicant referencing the LTR will be expected to revise and resubmit its respective documentation, or submit justification for continued applicability of the LTR without revision of the respective documentation.

Document transmitted herewith contains sensitive unclassified information. When separated from the enclosures, this document is "DECONTROLLED."

OFFICIAL USE ONLY – ENCLOSURE 2 CONTAINS PROPRIETARY INFORMATION

DC GEH - ESBWR Mailing List

(Revised 08/11/2010)

cc:

Ms. Michele Boyd  
Legislative Director  
Energy Program  
Public Citizens Critical Mass Energy  
and Environmental Program  
215 Pennsylvania Avenue, SE  
Washington, DC 20003

Mr. Tom Sliva  
7207 IBM Drive  
Charlotte, NC 28262

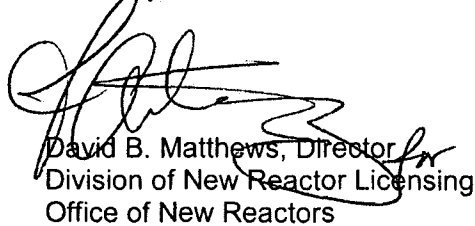
J. Head

- 2 -

Pursuant to 10 CFR 2.390, we have determined that the enclosed SE contains proprietary information. We will delay placing the non-proprietary version of this document in the public document room for a period of 10 working days from the date of this letter to provide you with the opportunity to comment on the proprietary aspects only. If you believe that any additional information in Enclosure 1 is proprietary, please identify such information line by line and define the basis pursuant to the criteria of 10 CFR 2.390.

The Advisory Committee on Reactor Safeguards (ACRS) subcommittee, having reviewed the subject LTR and supporting documentation, agreed with the staff's recommendation for approval following the May 18, 2010 ACRS subcommittee meeting.

Sincerely,



David B. Matthews, Director  
Division of New Reactor Licensing  
Office of New Reactors

Docket No. 52-010

Enclosure:

1. Safety Evaluation (Non-Proprietary)
2. Safety Evaluation (Proprietary)

cc: See next page (w/o enclosure)

## DC GEH - ESBWR Mailing List

### Email

aec@nrc.gov (Amy Cubbage)  
APH@NEI.org (Adrian Heymer)  
awc@nei.org (Anne W. Cottingham)  
bevans@enercon.com (Bob Evans)  
bgattoni@roe.com (William (Bill) Gattoni))  
BrinkmCB@westinghouse.com (Charles Brinkman)  
cberger@energetics.com (Carl Berger)  
charles.bagnal@ge.com  
charles@blackburncarter.com (Charles Irvine)  
chris.maslak@ge.com (Chris Maslak)  
CumminWE@Westinghouse.com (Edward W. Cummins)  
cwaltman@roe.com (C. Waltman)  
Daniel.Chalk@nuclear.energy.gov (Daniel Chalk)  
david.hinds@ge.com (David Hinds)  
david.lewis@pillsburylaw.com (David Lewis)  
David.piepmeyer@ge.com (David Piepmeyer)  
donaldf.taylor@ge.com (Don Taylor)  
erg-xl@cox.net (Eddie R. Grant)  
gcesare@enercon.com (Guy Cesare)  
GEH-NRC@hse.gsi.gov.uk (Geoff Grint)  
GovePA@BV.com (Patrick Gove)  
gzinke@entergy.com (George Alan Zinke)  
hickste@earthlink.net (Thomas Hicks)  
hugh.upton@ge.com (Hugh Upton)  
james.beard@gene.ge.com (James Beard)  
jerald.head@ge.com (Jerald G. Head)  
Jerold.Marks@ge.com (Jerold Marks)  
jgutierrez@morganlewis.com (Jay M. Gutierrez)  
Jim.Kinsey@inl.gov (James Kinsey)  
jim.riccio@wdc.greenpeace.org (James Riccio)  
joel.Friday@ge.com (Joel Friday)  
Joseph\_Hegner@dom.com (Joseph Hegner)  
junichi\_uchiyama@mnes-us.com (Junichi Uchiyama)  
kimberly.milchuck@ge.com (Kimberly Milchuck)  
KSutton@morganlewis.com (Kathryn M. Sutton)  
kwaugh@impact-net.org (Kenneth O. Waugh)  
lchandler@morganlewis.com (Lawrence J. Chandler)  
lee.dougherty@ge.com  
Marc.Brooks@dhs.gov (Marc Brooks)  
maria.webb@pillsburylaw.com (Maria Webb)  
mark.beaumont@wsms.com (Mark Beaumont)  
matias.travieso-diaz@pillsburylaw.com (Matias Travieso-Diaz)  
media@nei.org (Scott Peterson)  
mike\_moran@fpl.com (Mike Moran)

DC GEH - ESBWR Mailing List

MSF@nei.org (Marvin Fertel)  
mwetterhahn@winston.com (M. Wetterhahn)  
nirsnet@nirs.org (Michael Mariotte)  
Nuclaw@mindspring.com (Robert Temple)  
patriciaL.campbell@ge.com (Patricia L. Campbell)  
Paul@beyondnuclear.org (Paul Gunter)  
peter.yandow@ge.com (Peter Yandow)  
pshastings@duke-energy.com (Peter Hastings)  
rick.kingston@ge.com (Rick Kingston)  
RJB@NEI.org (Russell Bell)  
Russell.Wells@Areva.com (Russell Wells)  
sabinski@suddenlink.net (Steve A. Bennett)  
sandra.sloan@areva.com (Sandra Sloan)  
sara.andersen@ge.com (Sara Anderson)  
sfrantz@morganlewis.com (Stephen P. Frantz)  
stephan.moen@ge.com (Stephan Moen)  
steven.hucik@ge.com (Steven Hucik)  
strambgb@westinghouse.com (George Stramback)  
tdurkin@energetics.com (Tim Durkin)  
timothy1.enfinger@ge.com (Tim Enfinger)  
tom.miller@hq.doe.gov (Tom Miller)  
trsmith@winston.com (Tyson Smith)  
Vanessa.quinn@dhs.gov (Vanessa Quinn)  
Wanda.K.Marshall@dom.com (Wanda K. Marshall)  
wayne.marquino@ge.com (Wayne Marquino)  
whorin@winston.com (W. Horin)

FINAL SAFETY EVALUATION REPORT (SER) REVISION 1 FOR GE HITACHI NUCLEAR  
ENERGY LICENSING TOPICAL REPORT (LTR) NEDC-33326P REVISION 1, "GE14E FOR  
THE ECONOMIC SIMPLIFIED BOILING WATER REACTOR INITIAL CORE NUCLEAR  
DESIGN REPORT"

1 INTRODUCTION

The staff based its review of the nuclear design on information contained in Licensing Topical Report (LTR) NEDC-33326P (Reference 1), the Economic Simplified Boiling Water Reactor (ESBWR) design control document (DCD) (Reference 2), responses to staff requests for additional information (RAIs), and other supporting topical reports referenced by the applicant. The staff conducted its evaluation in accordance with the guidelines provided by Standard Review Plan (SRP) Section 4.3, "Nuclear Design."

2 REGULATORY CRITERIA

DCD Tier 2, Section 4.3, "Nuclear Design," presents the ESBWR nuclear design bases. The nuclear design must not exceed the specified acceptable fuel design limits during normal operation, including anticipated operational occurrences (AOOs), and the effects of postulated reactivity accidents will not cause significant damage to the reactor coolant pressure boundary (RCPB) or impair the capability to cool the core, or sustain unstable core conditions. To meet these objectives, the nuclear design must conform to the following general design criteria (GDC):

- GDC 10, "Reactor Design," requiring the reactor design (reactor core, reactor coolant system, control and protection systems) to assure that specified acceptable fuel design limits are not exceeded during any condition of normal operation, including AOOs.
- GDC 11, "Reactor Inherent Protection," requiring a net negative prompt feedback coefficient in the power operating range.
- GDC 12, "Suppression of Reactor Power Oscillations," requiring that power oscillations that can result in conditions exceeding specified acceptable fuel design limits are not possible, or can be reliably and readily detected and suppressed.
- GDC 13, "Instrumentation and Control," requiring a control and monitoring system to monitor variables and systems over their anticipated ranges for normal operation, AOOs, and accident conditions.
- GDC 20, "Protection System Functions," requiring, in part, a protection system that automatically initiates a rapid control rod insertion to assure that fuel design limits are not exceeded as a result of AOOs.
- GDC 25, "Protection System Requirements for Reactivity Control Malfunctions," requiring protection systems designed to assure that specified acceptable fuel design limits are not exceeded for any single malfunction of the reactivity control systems.



- GDC 26, "Reactivity Control System Redundancy and Capability," requiring, in part, a reactivity control system capable of holding the reactor subcritical under cold conditions.
- GDC 27, "Combined Reactivity Control Systems Capability," requiring, in part, a control system designed to control reactivity changes during accident conditions in conjunction with poison addition by the emergency core cooling system (ECCS).
- GDC 28, "Reactivity Limits," requiring, in part, that the reactivity control systems be designed to limit reactivity accidents so that the reactor coolant system boundary is not damaged beyond limited local yielding.

### 3 NUCLEAR DESIGN DESCRIPTION

#### 3.1 Summary of Technical Information

##### 3.1.1 Core Description

The topical report NEDC-33326P, (Reference 1) describes the ESBWR initial core design. The 4500 MWth ESBWR core consists of 1132 fuel bundles and 269 control blades. The core design given in Figure 3-1 of Reference 1 characterizes the initial full core design. Five types of fuel bundles, which are similar except for differences in enrichment and burnable poison content, are loaded in the reference pattern. Bundle differences allow for a flatter radial power distribution across the core and provide low reactivity bundles similar in the neutronic behavior to partially burnt bundles.

The applicant provided a description of the ESBWR fuel bundle designs including lattice information in Reference 1. The bundle designs included several zones that vary axially throughout the bundle. A two-dimensional lattice describes each zone. Multiple lattices describe the variation of the fuel bundle axially as the design includes part-length rods, vanished fuel rods<sup>1</sup>, variations in burnable poison loadings, and enrichment.

Typically, bundle nuclear properties in a core vary both axially and radially. As a result, the core is modeled with several nodes that account for these differences as well as the influence of individual nodes on the neighboring nodes. The staff safety evaluation report (SER) evaluates the modeling techniques and qualifications in References 3 and 4 for application to the ESBWR.

##### 3.1.2 Power Distribution

The acceptance criteria in the area of nuclear design, specifically power distributions, are based on meeting the relevant requirements of the GDC related to the reactor core and the reactivity control systems.

The nuclear design basis for control requirements is that maximum linear heat generation rate (MLHGR) and the minimum critical power ratio (MCPR) constraints shall be met during operation. The operating limit MCPR and MLHGR limit are determined such that the fuel rods do not exceed required licensing limits during AOOs.

---

<sup>1</sup> Vanished fuel rods refer to those rod locations within the bundle lattice above the part-length fuel rod plena. Within the bundle, at these specific rod locations and within this upper axial span there are no physical rods obstructing coolant flow.

### 3.1.3 Safety and Operating Limits

The MLHGR is the maximum local linear heat generation rate (LHGR), more specifically the fuel rod with the highest surface heat flux at any nodal plane in a fuel bundle in the core. The MLHGR operating limit is bundle-type dependent and the staff SER for LTR NEDC-33242P (Reference 5) evaluates the limit. The staff SER evaluates the LHGR, ensuring that it meets all mechanical design assumptions. The reactor cannot be operated with the fuel at LHGR values greater than acceptable values within the body of the safety analysis under normal operating conditions. Under abnormal conditions, including the maximum overpower condition, the MLHGR will not exceed the strain limit or cause fuel melting.

The MCPR is the minimum critical power ratio of all of the fuel bundles. The critical power ratio (CPR) for any bundle is the ratio of the bundle power that would result in transition boiling to the current bundle power. Therefore, the bundle with the smallest CPR has the smallest margin to transition boiling. The CPR is a function of several parameters; the most important are bundle power, bundle flow, the local power distribution and the details of the bundle mechanical design.

The plant operating limit MCPR (OLMCPR) is established by considering the limiting AOOs for each operating cycle. The OLMCPR determines that 99.9 percent of the rods avoid boiling transition during the limiting analyzed AOO, as discussed in the staff SER for LTR NEDC-33237P (Reference 6).

The design bases affecting power distribution of the ESBWR include the following parameters:

- Under abnormal conditions (including maximum overpower), the MLHGR will not exceed mechanical design limits for the fuel.
- The MCPR during normal operation will remain greater than the OLMCPR to avoid boiling transition during normal operation and AOOs.

GDC 13 provides the required criteria to evaluate core monitoring. In-core nuclear instrumentation performs core monitoring, in part, to ensure that the core operates within these limits. According to DCD Tier 2, Section 7.9, information from the core monitoring instrumentation is used by the 3D MONICORE system to determine the margin to operational limits. The 3D MONICORE system has two components, the Monitor and the Predictor. In each case, the calculational engine is the PANAC11 three-dimensional, quasi-steady-state core simulator. The staff's SER on References 3 and 4, discuss the analytical capabilities of the PANAC11 core simulator.

The 3D MONICORE system has several adaption methods. Adaption methods improve monitoring accuracy by incorporating live plant data from the neutron monitoring system in the core simulator.

The calculation of the bundle CPR and the nodal LHGR during operation are performed by the PANAC11 core simulator. 3D MONICORE reports the minimum bundle CPR and maximum nodal LHGR relative to their respective limits (OLMCPR and MLHGR limit, respectively). The thermal margin information is also passed to the automatic thermal limits monitor (ALTM), the rod worth minimizer (RWM) and the Multi-channel Rod Block Monitor (MRBM) subsystems of the rod control and information system (RC&IS). Instrumentation signals also inform the reactor

protection system (RPS). The RPS utilizes signals to initiate a reactor SCRAM when these signals exceed a specified setpoint.

#### 3.1.4 Neutron Monitoring System

Nuclear instrumentation monitors variables affecting the nuclear fission process. Appropriate controls ensure that the reactor operates within acceptable ranges. Specifically, the nuclear instrumentation monitors the reactor power and ensures that it does not exceed acceptable design limits. To meet these objectives, the nuclear design must conform to GDC 10 and 13.

The staff reviewed the nuclear instrumentation design in accordance with SRP Section 4.3. In DCD Tier 2 (Reference 2) and NEDE-33197P (Reference 4), the applicant describes how the instrumentation for power and power shape monitoring and calibration meets the requirements set forth in GDC 10 and GDC 13.

##### 3.1.4.1 Description of the Instrumentation

The ESBWR core monitoring is accomplished with several in-core nuclear instruments that cover the expected ranges for normal operation, AOOs, and accident conditions. The neutron monitoring system is comprised of three separate measurement systems: the source range monitor, the local power range monitor, and the automatic fixed in-core probe. The power range neutron monitoring system (PRNM) receives signals from several local detectors. These in-core nuclear instruments include the local power range monitors (LPRMs) as well as automatic fixed in-core gamma thermometers (GTs). For low powers characteristic of the source range through a normal startup (greater than 10 percent of rated thermal power) the source range neutron monitoring system (SRNM) monitors the core neutron flux.

The LPRMs are arranged in 64 strings, each with four detectors, and distributed throughout the core. The locations of LPRM strings are shown in Figure 7.2-7 of Reference 2. For every four by four array of bundles, there are four LPRM strings (one at each corner). The LPRM strings are comprised of four LPRM detectors that are spaced evenly axially throughout the core. The LPRM detectors are polarized fission chambers.

Inside the LPRM instrument guide tube, there are seven automatic fixed in-core probes (AFIP). The AFIP is a gamma thermometer instrument that is used to periodically calibrate the LPRM signal. Figure 7.2-8 of DCD Tier 2 (Reference 2) shows the axial elevation of the AFIPs. There are seven AFIPs in each LPRM instrument string. There is one AFIP at the same elevation as the midplane of each of the LPRM detectors. In between each LPRM detector there is another AFIP. The AFIPs are evenly distributed between the uppermost and bottommost LPRMs at 381 mm (15 inch) intervals for a total of seven AFIPs.

The neutron monitoring system instruments measure the neutron flux and monitor the fission process. The number and types of instruments included in the design are sufficient to monitor the flux over the entire range of operation between startup (low power), normal operation, and transient conditions (high power). When the reactor power is low, monitoring the startup process calls for increased instrument sensitivity. According to Chapter 7 of the DCD Tier 2 (Reference 2), the SRNM is comprised of 12 detectors. These detectors are fixed in-core regenerative fission chamber sensors. The 12 detectors are spaced evenly throughout the core and located at the core midplane axially; Figure 7.2-6, Reference 2, shows the radial locations.

The detectors are inside the pressure barrier tubes. The SRNM detectors measure the reactor flux over ten decades, from a flux level of approximately  $10^3$  n/cm<sup>2</sup>/sec to  $10^{13}$  n/cm<sup>2</sup>/sec. This range extends to approximately 10 percent of rated power. The LPRM monitoring capability overlaps this range as the LPRMs can monitor core power from the startup range through the power range: from one percent of power to greater than rated thermal power (Reference 2).

#### 3.1.4.2 Rod Control and Information System

The Rod Control and Information System (RC&IS) is a non-safety-related system. The RC&IS is a logic system that provides controls on reactor maneuvering through control rod motion during normal operation and maintains status information regarding the current control rod configuration for the reactor.

Using local power indications from the LPRM detectors, the RC&IS subsystems issue rod blocks to ensure that control rod motion does not exceed safety and operating limits. The ATLM and MRBM work together above the low power set point to inhibit rod withdrawals when local detectors indicate power changes that challenge the MLHGR limit or the OLMCPR. The MRBM, unlike conventional rod block monitors, uses several channels of LPRM indications throughout the core to simultaneously monitor each region of the core where control rods are being withdrawn during ganged withdrawal sequences. Below the low power set point, the RWM compares the sequence to withdraw the control rod at low power to a preprogrammed control rod withdrawal pattern. In cases where the control rod's withdrawal is different, the RWM enforces control rod insertions and withdrawals at low power to reduce the available reactivity worth of a control rod to mitigate the consequences of a control rod drop accident during low power operation (Reference 2).

Upon receipt of a SCRAM signal by the RPS, the RC&IS initiates a fast fine motion control rod drive (FMCRD) run-in as a backup to the hydraulic SCRAM through the diverse protection system (DPS). The RC&IS also sends selected control rod run-in (SCRRI) signals to the DPS following specific AOOs, namely load rejection, turbine trip and loss of feedwater heating (Reference 2).

Another important function of the RC&IS is to interface with the plant computer to perform LPRM calibration and plant simulator adaption. This function is performed by using AFIP signals in conjunction with three dimensional nuclear models to determine gain adjustments and nodal parameter corrections. The AFIP signals are input into the 3D MONICORE system to perform adaption. The staff's SER on References 3 and 4 evaluate the calibration and adaption features of 3D MONICORE with the ESBWR specific AFIP design.

#### 3.1.5 Reactivity Coefficients

The reactivity coefficients express the effects of changes in the core conditions, such as power, fuel and moderator temperature, and moderator density, on core reactivity. These coefficients vary with fuel exposure and power level. The applicant has provided calculated values of the coefficients in Reference 1.

Reactivity coefficients, the differential changes in reactivity produced by differential changes in core conditions, use external disturbances to predict the response of the core. The base initial condition of the system and the postulated initiating event determine which of the several defined coefficients are significant in evaluating the response of the reactor. The coefficients of interest are the Doppler coefficient, the void reactivity coefficient, and the moderator temperature coefficient. The combination of these reactivity coefficients dictates the power

reactivity coefficient. A combination of negative coefficients ensures that the reactor will have an inherent negative reactivity feedback with increasing power.

Reference 3 evaluates the computational tools employed by the applicant to calculate the reactivity coefficients. The coefficients calculated by the applicant are not used in steady state or transient analyses, but are meant to demonstrate compliance with GDC 11.

#### 3.1.5.1 Doppler Reactivity Coefficient

In order to demonstrate that the Doppler reactivity coefficient remains negative in the power operating range, the applicant calculated temperature dependent eigenvalues for each of the five fuel bundle types for the dominant zone lattice. At each point in exposure, the temperature was increased and the change in eigenvalue was shown to be negative at all points in exposure. The Doppler reactivity coefficient is predominantly driven by the uranium-238 and plutonium-240 content in the fuel and, while an inherent feature of the fuel, this coefficient does not vary significantly among BWR fuel designs. The ESBWR initial core calculated Doppler coefficient is approximately  $[-0.0015 \text{ per } \Delta T]$ , which is slightly greater (in magnitude) than typical values of operating reactor Doppler coefficients. The applicant attributes the difference to a lower initial enrichment (Reference 1).

#### 3.1.5.2 Void Reactivity Coefficient

The applicant estimated the void reactivity coefficient for both the power range of operation and for cold shutdown conditions. The applicant's analyses indicate a negative trend of core eigenvalue with increasing core average void content in the power range of operation, indicating inherent negative reactivity feedback under these conditions. The magnitude of the void reactivity coefficient, however, decreases with decreasing void content. Therefore, the applicant identified the cold shutdown condition as a limiting case, particularly at the end of the cycle following depletion of burnable poisons. The end of cycle conditions are typically over-moderated and, given that the core is entirely fresh, there are no significant plutonium driven spectral effects. The analysis for the limiting condition verifies that the void reactivity coefficient is negative. The value of the coefficient is calculated to be about  $[-0.0015 \text{ per } \Delta V]$  at the most limiting condition (Reference 1).

#### 3.1.5.3 Moderator Temperature Coefficient

Lastly, the applicant calculated the moderator temperature coefficient. During normal operation, the coolant is only subcooled near the core inlet and remains at a near constant temperature once reaching saturated conditions. The end of the reference cycle was identified as the condition with the least negative moderator temperature coefficient. The results indicate that at temperatures above  $[250^\circ\text{F}]$  the core eigenvalue decreases with increasing water temperature (Reference 1).

The moderator temperature coefficient decreases in magnitude over cycle exposure with the withdrawal of control rods and the depletion of gadolinia burnable poisons. Late in the cycle, the reduction in the poison content leads to potential conditions where the reactor is over-moderated, thereby yielding a positive moderator temperature coefficient for cold conditions. While the end of cycle (EOC) moderator temperature coefficient is positive, it is small compared to the effects of the void reactivity feedback. The applicant's calculations show that the

moderator temperature coefficient at the EOC may be positive and on the order of [[  
]] (Reference 1).

### 3.1.6 Control Requirements

The control rod system is designed to provide shutdown margin and reactivity control of maximum excess reactivity anticipated during cycle operation. The control rods provide reactivity changes that compensate for the reactivity effects of the fuel and water density changes accompanying power level changes over the range from full load to no load and allow for control of the power distribution within the core.

The reference rod patterns for the ESBWR core are similar to current BWR rod patterns. For the first half of the cycle, burnable poisons in conjunction with a conventional rod pattern control the hot excess reactivity. During the middle of the cycle, very little rod movement is needed because of a nearly constant hot excess reactivity during this part of the cycle. In the latter part of the cycle the other half of the rods are employed in a similar checkerboard pattern. During the progression towards the EOC the control rods in the second set are withdrawn, and finally the first set is used for control towards the EOC where there is just a small amount of hot excess reactivity.

This reference rod pattern is used in the analyses of the core power distribution and is an input into the Chapter 6 and 15 analyses that describe accidents and transients starting from different times during cycle operation. The reference rod pattern for the initial cycle also factors into the determination of the radial and axial power distributions in the core. As is common for currently operating BWRs, the axial power shape is bottom peaked at the beginning of cycle (BOC) and evolves into a slightly top peaked distribution at the EOC.

Margins to thermal operating limits (Maximum Fraction of Limiting Power Density and the CPR Ratio) were analyzed over the initial operating cycle.

In addition to providing the means for controlling core reactivity for power maneuvering, the control rods provide the minimum shutdown margin following any AOO and are capable of making the core subcritical rapidly enough to prevent exceeding specified acceptable fuel design limits. The control rods automatically insert hydraulically upon receipt of a SCRAM signal from the reactor protection system.

The applicant has provided an analysis in Figure 3-44 of Reference 1 showing that the control rod worth is sufficient to ensure a subcritical configuration for xenon-free, cold shutdown conditions at the beginning of the cycle. The BOC condition is often limiting in terms of available shutdown margin. The analysis presented indicates a minimum shutdown margin of [[  
]] at the BOC.

The applicant provided analyses of the shutdown margin for the reactor during several points in exposure. At the beginning, middle, and end of cycle (BOC, MOC, and EOC) exposure points, the applicant calculated the shutdown margin assuming one control rod withdrawn, and repeated the calculation for each control rod. Therefore, this calculation identifies the highest worth control rod at each exposure point, the shutdown margin with the highest worth rod withdrawn, and the relative worth of the remaining control rods. As is expected, the shutdown margins are greatest when the low worth peripheral rods are stuck out. During cycle exposure, the core radial power shape tends to shift outward, and this is consistent with decreasing shutdown margins assuming stuck-out control rods near the core edge towards EOC.

The control rods are backed up by the standby liquid control system (SLCS). The SLCS is a second reactivity control system meant to provide a diverse and redundant capability to the control rods. The SLCS is an accumulator-driven boron injection system. The SLCS is designed to provide the capability of bringing the reactor, at any time in a cycle, from full power with a minimum control rod inventory (which is defined to be at the peak of the xenon transient) to a subcritical condition with the reactor in the most reactive xenon-free state if the control rods fail to insert.

The applicant analyzed the capability of the SLCS system to inject sufficient boron into the reactor coolant system so that the resultant equivalent uniform boron concentration ensures that the reactor is subcritical (with [[                    ]] margin) under cold shutdown, xenon-free conditions from its most critical state with the control rods fully withdrawn.

### 3.1.7 Stability

GDC 12 requires that power oscillations that could result in exceeding the specified acceptable fuel design limits be prevented or readily detected and suppressed.

DCD Tier 2, Section 4.3.3.6, "Stability Evaluation," discusses the stability of the reactor with respect to xenon-induced power distribution oscillations. The strong negative reactivity feedback from the void reactivity coefficient damps xenon-induced power distribution oscillations. The applicant presented considerations of thermal-hydraulic stability in DCD Tier 2, Appendix 4D for the equilibrium core. The staff evaluation addresses the thermal-hydraulic stability of the ESBWR equilibrium core in SER Section 4A and for the initial core in the staff safety evaluation report for NEDO-33337 (Reference 7).

In NEDO-33337, the applicant references an approved NRC methodology for performing stability analyses. The approval of the methodology, as described in Reference 8, however, is contingent upon demonstrating accuracy in the PANACEA provided cross sections to the TRACG 3D kinetics model. The staff's SER evaluates the efficacy of the nuclear design methodology in Reference 3. Approval of NEDC-33239P constitutes approval of PANAC11 to generate nuclear data for use by TRACG04.

### 3.1.8 Reactivity Accidents

GDC 28 requires that the reactivity control system be designed in such a way as to preclude reactivity accidents of sufficient magnitude to impair core coolability or reactor coolant pressure boundary (RCPB) integrity.

The consequences of a postulated control rod drop accident are sensitive to the core management loading and specific core design. Factors such as control blade worth and radial power peaking are key parameters in assessing the consequences of such an accident. Therefore, the staff requested in RAI 4.6-38 that GEH evaluate the consequences of a control rod drop accident for the initial core design.

The response to RAI 4.6-38 refers to the analysis performed in response to RAI 4.6-23, Supplement 2. The response briefly describes a reload licensing screening approach, analysis procedures, and analytical results. The analyses were performed using the PANAC11 (PANACEA version 11) three dimensional simulator in a transient mode with six delayed neutron groups. PANAC11 calculates the fuel enthalpy rise according to an adiabatic model (by

integrating transient power) and explicitly accounts for blade worth, nominal blade pull during startup, and radial power shapes.

Calculated fuel enthalpy rise for the ESBWR initial core design indicates significant margin to the interim criteria in SRP Section 4.2, Revision 3. The maximum calculated fuel enthalpy rise for the initial core is [[ ]]. The limiting enthalpy rise is for the BOC for a static blade worth of [[ ]] (Reference 9). For low exposure the cladding failure fuel enthalpy rise limit is [[ ]]. The initial core CRDA analysis indicates significant margin to cladding failure. Therefore barrier integrity is ensured as the analysis indicates that no fuel rods fail. The radiological consequences of such an accident are bounded by the analyses in DCD Section 15.3.1.5, which is based on 1000 failed fuel rods (Reference 2).

#### 4 STAFF EVALUATION

The applicant provided several analyses to demonstrate ESBWR initial core compliance with the prescribed GDC in SRP Section 4.3. The staff's SER on References 3 and 4 reviews the results of these analyses in the following sections.

The staff evaluated the information contained in the subject LTR and supporting topical reports as it relates to ESBWR design compliance with GDC 10, 11, 12, 13, 20, 25, 26, 27 and 28. The staff described the review of the applicant's analyses in the following sections as they relate to concerns regarding power distribution and operating limits, reactivity feedback, and reactivity control. The staff reviewed compliance with GDC 12 as it relates to thermal hydraulic stability in its review of the initial core transients, LTR NEDO-33337 (Reference 7).

##### 4.1 Power and Operating Limits

As set forth above, GDC 10 and 13 specify the requirements for the core operating power and instrumentation.

The MLHGR limit and OLMCPR are determined such that operation within these limits prevents fuel damage from melting, excessive strain, or boiling transition. These limits are determined such that there is adequate margin to account for the effects of AOOs. The staff documented the review of the methods for determining the MLHGR limit and the OLMCPR in the staff's safety evaluation of References 6 and 7 respectively. Operation by the 3D MONICORE system based on fuel specific analyses, the PANAC11 computational engine, and plant instrumentation determine the limits. The uncertainties in the methodology and plant instrumentation are addressed in the NRC approved methodologies (References 3, 4, 7, 10, 11, and 12). In its review the staff considered the modifications made to the methods for expanded operating domains (Reference 18) and their applicability to the ESBWR operating conditions. The staff also considered aspects of the methods unique to the ESBWR plant instrumentation (Reference 4). In response to staff RAI 4.4-68, the applicant verified that the bundle R-factor is determined using limiting axial power and void fraction profiles (Reference 13). The staff reviewed these profiles and finds them acceptable for determining a conservative R-factor for the initial core. The staff's SER on References 3 and 4 describes the review of the incorporation of uncertainties into the limits.

The staff reviewed the nuclear design performance over the initial cycle, as analyzed by the applicant. The methods for determining the margin to limits are described in NEDC-33237P, NEDC-33242, and NEDC-33239P (which references NEDE-33197P). The staff acceptance of



the uncertainties and methodology will be documented in the staff's safety evaluation of NEDE-33197P, NEDC-33239P, NEDC-33237P, and NEDC-33242P. The cycle analysis performed by the applicant shows that the reference loading pattern and control rod withdrawal sequence for the ESBWR indicate that there is margin to both of these limits during normal operation.

To account for the effects of AOOs, the applicant provided analyses demonstrating the capability of the reactor protection system (RPS) and associated control rod system to perform its SCRAM function in NEDO-33337. The staff documented its evaluation of NEDO-33337 in the staff's DCD SER Section 15. The automatic function of the RPS is to prevent exceeding acceptable fuel design limits in the event of AOOs.

The applicant bases its analyses on the actuation of the RPS in response to input signals in excess of a setpoint value. The applicant provided a description of the methodology for the determination of setpoints. The determination process includes margin associated with uncertainties in the instrumentation. The staff's evaluation of the setpoint methodology is provided in Chapter 7 of the staff's safety evaluation of the ESBWR DCD.

The applicant's cycle calculations show adequate margin to both the MLHGR and OLMCPR limits during normal operation, and evaluated the function of RPS to SCRAM the reactor prior to exceeding any specified acceptable fuel design limits (SAFDLs). Therefore, the staff approval of NEDO-33337 in conjunction with the information provided in Reference 1 sufficiently demonstrates compliance with GDC 10.

#### 4.2 Neutron Monitoring

The neutron monitoring system is designed to meet the requirements of GDC 13. Specifically the PRNM and SRNM are designed to monitor the fission process over the range of anticipated operation and accident conditions. The PRNM is comprised of several LPRM detectors with the capability of monitoring the neutron flux in the reactor between one percent of rated core power and well over 100 percent of the rated core power (125 percent). The SRNM is designed to monitor the neutron flux at very low levels ( $\sim 10^3$  n/sq-cm/sec) or approximately 10 decades below the normal operating level. The combination of these two neutron monitoring subsystems allows for an overlapping monitoring capability over the full range of neutron flux levels under normal operation including startup and anticipated operational occurrences. The LPRM capability extends to higher neutron flux levels allowing for monitoring of the reactor core power during accident conditions and anticipated transients without SCRAM. Therefore, the staff finds that the ESBWR neutron monitoring system is acceptable in that it provides sufficient capability and adequately monitors the neutron flux levels in the reactor over the necessary ranges.

The in-core ESBWR neutron monitoring system is based on a series of distributed local power range monitors. Substantially, the polarized fission gas chambers are the same as those instruments widely applied within the operating fleet of BWRs. The design differences between the ESBWR and conventional BWRs will not impact the fundamental operation of the LPRMs so long as the steady state bypass void fraction remains below 5 percent. These instruments interface with the 3D MONICORE system to determine the operating characteristics of the core.

The neutron monitoring system includes in-core gamma thermometers (GTs) replacing the function of the traversing in-core probe (TIP) system for conventional reactors. The gamma thermometers determine, much as gamma TIP instruments do, the axial power shape based on local gamma flux indications. There are two primary differences between the gamma TIP and

GT instruments. First, the GT instrument operates by inferring the local gamma flux based on heat deposition in the instrument. Second, the GTs do not move through the core.

The staff reviewed the information provided by the applicant in regard to the GT design and found that with regular calibration the GT can be used to determine the local gamma flux. When combined with coupled transport calculations to determine the detector response kernels (or signal to power ratios) the GT indication may adequately determine the local nodal power in surrounding nodes. The GT instruments are spaced within the core alongside the LPRMs, giving a complete radial mapping capability if the core power distribution is quadrant symmetric.

The 3D MONICORE system determines the margin to limits based on input from the neutron monitoring system, adaption, and input from the core thermal hydraulic instrumentation (i.e. core flow). The 3D MONICORE system is based on the PANAC11 calculational engine. The staff's SER on References 3 and 4 documents staff review of the PANAC11 code.

However, GDC 13 also requires that appropriate controls are in place to ensure that the reactor core is operated within prescribed safety and operating limits. The GDC 13 requirements for the NMS are fulfilled by prescribing limits that account for instrument and measurement uncertainties. Of key importance to the prescription of these limits is the accuracy of the neutron flux measurements. The pedigree of LPRM measurements in particular is related to the efficacy of the AFIPs and process computer to effectively and accurately calibrate the local indications of the neutron flux level. Additionally, the core monitoring system is used to adapt predictive calculations performed by the 3D MONICORE system to determine the local power distribution. The staff's SER for References 3 and 4 describes the reviewed and evaluated methods used to account for any uncertainties in the measurement, calibration, and adaption of the core neutronic modeling in the MLHGR limit and OLM CPR.

Therefore, the in-core instrumentation meets the requirements of GDC 13 by providing monitoring capability over the range of expected operation and providing sufficient information, given the capabilities of the 3D MONICORE system, to monitor core operating parameters relative to associated operating limits.

The staff finds that the ESBWR initial core design adequately meets the requirements of GDC 10 and 13, and is therefore acceptable.

#### 4.3 Reactivity Feedback

As set forth above, GDC 11 requires that the core be designed with inherent negative reactivity feedback.

The applicant provided several analyses to indicate the nature and magnitude of the reactivity feedback coefficients for the reference ESBWR core. The staff's SER on References 3 and 4 reviewed the applicant's nuclear methods. In each case the applicant performed the analysis by perturbing the steady state calculation to determine the change in eigenvalue as a result of a change in the fuel temperature, coolant temperature, or coolant void.

In general, the Doppler coefficient is a strong function of fertile heavy metal content and spectrum hardness. For the ESBWR, the enrichment and planar fuel geometry are similar to operating BWRs. However, the bundle enrichment is slightly lower and the bundle pitch is slightly greater. The greater pitch and lower enrichment soften the neutron spectrum. A softened spectrum reduces the fertile resonance integral and consequently would serve to

reduce the Doppler coefficient in magnitude. However, the reduced enrichment results in a smaller positive reactivity effect from enhanced fissile resonance absorption. The net effect of these differences is an increase in the Doppler coefficient magnitude. The applicant's calculations are consistent with this expectation.

The increased assembly spacing also affects the moderator temperature coefficient. The increased hydrogen to heavy metal ratio decreases the magnitude of the moderator temperature coefficient and leads to slightly positive values for cold (zero power) conditions at the EOC where the neutron spectrum is very soft (thus, over-moderated). The positive nature of the moderator temperature coefficient is of minor concern, due to the relatively slow nature of the moderator temperature change (relative to fuel temperature change), and, at normal operating conditions, the core dynamic behavior is driven predominantly by the strong, negative void reactivity feedback. This condition is only for low temperatures and is not of sufficient magnitude to cause operational concerns during startup and shutdown operations, or a reactivity insertion problem.

The applicant provided a series of core calculations to determine the estimated void coefficient. As the void reactivity coefficient is stronger for higher void fractions, the applicant performed calculations for cold shutdown conditions. This calculation is conservative because the spectrum at cold shutdown conditions is over-moderated. The applicant simulated the effects of voids in the subcooled coolant using the PANAC11 core simulator, and found that in the most limiting case the void reactivity coefficient was negative.

The power reactivity coefficient is a combination of the Doppler, void, and moderator temperature reactivity coefficients. While the design differences of the ESBWR make the moderator temperature and Doppler coefficients less negative than for an operating BWR, the increased void, higher enrichment, and higher burnable poison loading result in an overall negative power coefficient. In the case of the ESBWR, the void coefficient is not significantly different from operating reactors and a dominant contributor to the power coefficient. The staff finds these values for the reactivity coefficients to be acceptable because they are negative in the power operating range, ensure a negative power reactivity coefficient, and therefore meet the requirements of GDC 11.

#### 4.4 Reactivity Control

As set forth above, GDC 20, 25, 26, 27, and 28 specify the requirements for the reactivity control systems.

The reactivity control worth calculations were performed using the TGBLA06 and PANAC11 codes. These calculations show that the rod values are similar to operating BWR control rod worth. For the middle of the ESBWR initial cycle the hot excess reactivity is nearly constant, therefore requiring a high in-core rod density during normal operation near the beginning of cycle. The beginning of cycle hot excess is comparable to the peak hot excess and the neutron spectrum is the hardest (due to the presence of large quantities of burnable absorber), limiting individual control rod worth. Therefore, this condition is limiting as the additional available rod density for control is small and each rod worth is relatively low compared to other points during cycle exposure. By demonstrating shutdown margin with the strongest control rod withdrawn in the limiting condition, the applicant has demonstrated the system can fully control the core reactivity given the failure of a single control rod to insert.

Additionally, the applicant calculated the shutdown margin at several exposure points during the cycle to demonstrate that the BOC condition is the limiting point. Towards the EOC the shutdown margin decreases, due to the buildup of plutonium and depletion of burnable poisons leading to an increase in the hot excess over the course of the cycle. However, the increase in the hot excess is sufficiently small such that the shutdown margin at the BOC is the most limiting.

On this basis, the staff determined that the control system has adequate negative reactivity worth to ensure shutdown capability, assuming that the most reactive control rod is stuck in the fully withdrawn position.

The control rod system automatically inserts control blades to shut down the reactor on receipt of a SCRAM signal. The negative reactivity worth of the control rods is sufficient to bring the reactor to a cold shutdown condition at any point during exposure. The staff's SER for Chapters 7 and 15 of the ESBWR DCD for LTR NEDO-33337 document the staff review of the RPS design to adequately prompt automatic control rod insertion during AOOs. Therefore, the design meets the requirements of GDC 20.

Additionally, control rod assignments to particular hydraulic control units shall maintain sufficient distance between rods such that there is essentially no neutronic coupling between the control cells, such that there is no significant impact on the shutdown margin given a failure of a single hydraulic control unit. When the reactor is shut down, the core is filled with liquid water and the mean free paths for neutrons are much smaller than at power, where the presence of voids allows for increased neutron transport during slowing down. Therefore, control cell neutronic coupling is effectively limited to nearby neighboring control cells. The assignment of control rods to hydraulic control units, such that no hydraulic control unit drives two nearby control rods would preclude neutronic coupling. Without any coupling, there is no synergistic effect of a dual control rod insertion failure which could result in local criticality. The HCU mapping is provided in Reference 1. The HCU mapping indicates that the control rods assigned to a specific HCU are distanced apart from each other within the core. The mapping indicates that the distance between control rods sharing an HCU is between five and seven control rod locations. As the mean free path for even higher energy neutrons at normal operating conditions ranges of about 15 - 30 cm, and the mean free path is reduced when the core is under cold conditions with control rods inserted, the staff finds that the HCU assignments adequately preclude the possibility of synergistic reactivity effects. Therefore, local criticality based on the failure of any particular HCU is not a concern if the remainder of the control rods inserted provide sufficient negative reactivity to ensure that the reactor is shut down and subcritical under cold conditions at its most reactive point.

The staff considered the design basis cold critical eigenvalue that is used to determine the analytical shutdown margin. The initial core nuclear design predicted shutdown margin is very large ([ ] at the limiting exposure point). This margin well exceeds the design requirement of 1 percent and includes sufficient additional margin to bound (with 95 percent confidence) the variability in cold critical eigenvalue (based on operating fleet experience) without consideration of the bias. In response to RAI 4.3-11, the applicant provided a qualification of the startup cold eigenvalue design basis against Plant A (a large BWR/4 restart core with modern (GE14) fuel) (Reference 13). The results indicate that the BOC and mid-cycle eigenvalues are conservative relative to the design basis and trend similarly with standard reload eigenvalue bases. The staff therefore finds that the shutdown margin is sufficiently large to provide reasonable assurance that the requirements of GDC 25 are met considering the failure of a single rod to insert.

The DCD Tier 2 in Section 4.3.1.2 and Appendix 4B state that compliance with GDC 26 is demonstrated by showing margin to criticality in the most reactive cold condition with the strongest rod pair withdrawn. The applicant provided the assignment of control rods to individual HCUs in Section 4.3.3 of the DCD Tier 2 (Reference 2). The staff has evaluated the calculation of the shutdown margin and reactivity margin to criticality at cold conditions assuming the strongest rod pair withdrawn. The staff finds that the shutdown margin

calculations in NEDC-33326P provide reasonable assurance that the requirements of GDC 26 are met.

The SLCS meets the requirements for diverse and redundant control systems per GDC 26 and the combined reactivity control system requirements per GDC 27. The staff has determined that the SLCS is adequate for bringing the reactor to a cold shutdown condition at any point in exposure, and therefore acts as a fully redundant control system. The system is diverse in that it is a dissolved-poison, passive, liquid injection system, thereby adequately satisfying GDC 26. As the SLCS is fully capable of controlling the reactivity and is an emergency core cooling system, it provides sufficient negative worth to compensate for a partial failure of the control rod system, thereby adequately satisfying GDC 27. The analysis indicates a very large margin (~9 percent). The margin is sufficiently large that it ensures subcriticality considering any additional uncertainty in the determination of the cold critical eigenvalue (maximum uncertainty of ~0.5 percent).

Compliance with GDC 28 is demonstrated by analysis of the consequences of a postulated control rod drop accident. The staff notes some conservatism in the initial core analysis, in particular the adiabatic assumption precludes any void formation (which would insert negative reactivity during the accident). Also, the calculations are performed assuming that the worth of the dropped rod, regardless of its position during the startup withdrawal sequence, is added to a critical reactor.

The analysis appropriately assumes that the control rod is dropped from its full inserted position to the position of the drive and accounts for the effects of exposure explicitly.

The staff notes that neither operator error nor calculational biases and uncertainties were included in the calculation. The staff, however, has reviewed the applicability of PANAC11 to evaluating nuclear characteristics for the ESBWR in its review of Reference 8. The staff found that PANAC11 is suitable for calculations of blade worth for the ESBWR. The staff approved previous versions of PANACEA to provide control blade worth and control rod drop shape information to downstream transient evaluations (References 14, 15, 16, and 17). Therefore, the staff is reasonably assured that the calculations are indicative of the expected ESBWR behavior; however, the staff does not find that the brief description of the reload licensing methodology for CRDA is adequate for staff review for generic application to all ESBWR reload licensing evaluations. Therefore, the staff's acceptance of the analytical CRDA results for the initial core design does not constitute staff approval of the reload licensing methodology for CRDA outlined in the RAI response generically.

The staff found that the low enthalpy rises are a result of low blade worth (less than 80 cents in all cases). Therefore, the staff finds that the calculational results indicating large margin are expected. There is reasonable assurance that consideration of modeling biases, uncertainty, and operator error would not result in changes to the analytic result on the order of magnitude of the available margin. The large margins to cladding failure for the ESBWR initial core provide

the staff reasonable assurance that, for the core design described in the subject LTR, the radiological consequences are bounded by the DCD analyses and that barrier integrity has been demonstrated.

On the basis of its review of the information provided in NEDC-33326P, as described above, the staff concludes that the functional design of the ESBWR reactivity control systems meets the requirements of GDC 20, 25, 26, 27 and 28 and, therefore, is acceptable

#### 4.5 Stability and Transient Calculations

The applicant provided extensive analyses demonstrating that the ESBWR is not susceptible to xenon-induced power oscillations in Reference 3. The staff has found that the ESBWR, generally, is not susceptible to xenon-induced power oscillations due to the strong void power coupling through the void reactivity coefficient. Therefore, the staff finds that the ESBWR compliance with GDC 12 need only consider thermal hydraulic instability.

The review of References 3 and 4 is documented in the associated staff SER, which addresses the acceptability of the use of the nuclear design methodology to provide information to the transient reactor analyses.

The staff reviewed the results of the stability analyses in DCD, SER Section 4A for LTR NEDO-33337 (Reference 7).

#### CONCLUSION

To allow for changes in reactivity from reactor heat up, changes in operating conditions, fuel burnup, and fission product buildup, the applicant has designed a significant amount of excess reactivity into the core. The applicant provided substantial information about core reactivity balances for the initial cycle, and has shown that the design incorporates methods to control excess reactivity at all times. The applicant has shown that sufficient control rod worth would be available at any time during the cycle to shut down the reactor, assuming that the most reactive control rod is stuck in the fully withdrawn position.

The applicant's assessment of reactivity control requirements over the initial cycle is suitably conservative, and the control system has adequate negative worth to ensure shutdown capability.

With respect to the requirements applicable to the nuclear design of the ESBWR, the staff finds the following:

- The applicant has satisfied the requirements of GDC 10, 20, and 25 with respect to fuel design limits by demonstrating that the ESBWR design meets the following objectives:
  - No fuel damage occurs during normal operation, including the effects of AOOs (GDC 10).
  - Automatic initiation of the reactivity control system ensures that fuel design criteria are not exceeded as a result of AOOs and those systems and components important to safety will automatically operate under accident conditions (GDC 20).

- No single malfunction of the reactivity control system will violate the fuel design limits (GDC 25).
- The staff reviewed the results of the applicant's calculations with respect to the Doppler, void, and moderator coefficients of reactivity are negative in the power operating range. The calculations indicated the relative magnitude of the coefficients and nature. They are generally similar to operating BWRs. Accordingly, the applicant has satisfied the requirements of GDC 11 with respect to nuclear feedback characteristics.
- The staff reviewed the applicant's analysis of xenon-induced power oscillations and has determined that the analysis is suitably conservative and performed with appropriate ESBWR inputs. Furthermore, the staff has evaluated how nuclear parameters are translated into TRACG through PANACEA, and finds this method acceptable. Therefore, the staff concluded that xenon-induced power oscillations are not a concern in the requirements of GDC 12, and the PANACEA Wrap-up file is adequate for the purposes of calculating reactor kinetic behavior for stability analyses. The acceptability of the design in terms of GDC 12 is addressed in the staff's SER for LTR NEDO-33337 in regard to thermal-hydraulic instabilities.
- The staff reviewed the applicant's core monitoring system, and finds that the applicant has satisfied the requirements of GDC 13 by providing instrumentation and controls to monitor the fission process. The applicant has also demonstrated the ability of the PANAC11 calculational engine to acceptably determine the margin to safety limits based on plant live data.
- The ESBWR design includes a standby liquid control system, which provide the following capabilities:
  - Reliable shutdown of the reactor during normal operating conditions and during AOOs in the event of multiple failures in the control rod drive system
  - Adequate boron injection capability to maintain safe-shutdown at all times during the reference cycle.

Accordingly, the staff concludes that the applicant has satisfied the requirements of GDC 26 by providing two independent reactivity control systems of different design and GDC 27 by including a system that injects dissolved absorber through the accumulator driven SLCS.

- The ESBWR control rod system design includes many design features to limit the possibility of a control rod drop accident. Calculations were performed that demonstrate that there are no fuel cladding failures as a result of a postulated control rod drop accident for the initial core design. Therefore, the requirements of GDC 28 are met.

For the reasons set forth above, the staff concludes that the ESBWR nuclear design satisfies the requirements of GDC 10, 11, 13, 20, 25, 26, 27 and 28, and therefore is acceptable.

## References

1. NEDC-33326P, Revision 1, *GE14E for the ESBWR Initial Core Nuclear Design Report*, General Electric-Hitachi, March 2009. (ADAMS Accession No. ML090970809)
2. ESBWR Design Control Document Tier 2, Revision 4. (ADAMS Accession No. ML072900480)
3. NEDC-33239P, Revision 0, *GE14 for ESBWR Nuclear Design Report*, Global Nuclear Fuels, February 2006. (ADAMS Accession No. ML060540345), as revised: NEDC-33239P, Revision 4, *GE14 for ESBWR Nuclear Design Report*, Global Nuclear Fuels, March 2009. (ADAMS Accession No. ML090970167)
4. NEDE-33197P, *Gamma Thermometer System for LPRM Calibration and Power Shape Monitoring*, General Electric, September 2005. (ADAMS Accession No. ML052700451)
5. NEDC-33242P, *GE14 for ESBWR Fuel Rod Thermal-Mechanical Design Report*, Global Nuclear Fuels, January 2006. (ADAMS Accession No. ML070870598)
6. NEDC-33237P, *GE14 for ESBWR - Critical Power Correlation, Uncertainty, and OLMCPR Development*, Global Nuclear Fuels, March 2006. (ADAMS Accession No. ML060750695)
7. NEDO-33337, *ESBWR Initial Core Transient Analysis*, General Electric-Hitachi, October 2007. (ADAMS Accession No. ML0728509420)
8. NEDE-33083P, Supplement 1, *TRACG Application for ESBWR Stability Analysis*, General Electric, December 2004. (ADAMS Accession No. ML050060161)
9. MFN-08-350, Kinsey, J., General Electric – Hitachi, Letter to the US Nuclear Regulatory Commission, "Response to Portion of NRC Request for Additional Information Letters No. 115 and No.137 – Related to ESBWR Design Certification Application – RAI Numbers 4.6-23 Supplement 2 and 4.6-38, Respectively," April 14, 2008. (ADAMS Accession No. ML081090147)
10. NEDC-32694P-A, *Power Distribution Uncertainties for Safety Limit MCPR Calculations*, General Electric, August 1999. (ADAMS Accession No. ML003740151)
11. NEDC-32601P-A, *Methodology and Uncertainties for Safety Limit MCPR Evaluations*, General Electric, August 1999. (ADAMS Accession No. ML003740145)
12. Watford, G. A., General Electric, letter to U.S. Nuclear Regulatory Commission, "Confirmation of the Applicability of the GEXL14 Correlation and Associated R-Factor Methodology for Calculating SLMCPR Values in Cores Containing GE14 Fuel," FLN 2001-017, October 1, 2001. (ADAMS Accession No. ML012830075)
13. MFN-08-087, Kinsey, J., General Electric – Hitachi, Letter to US Nuclear Regulatory Commission, "Response to Portion of NRC Request for Additional Information Letter No. 137 – Related to ESWR Design Certification Application – RAI Numbers 4.3-11 and 4.4-68," February 4, 2008. (ADAMS Accession No. ML080380296)



14. NEDO-10527 Supplement 2, *Rod Drop Accident Analysis for Large Boiling Water Reactors: Addendum No.2 Exposed Cores*, General Electric, January 1973. (ADAMS Accession No. ML081140547)
15. NEDO-10527, *Rod Drop Accident Analysis for Large Boiling Water Reactors*, General Electric, March 1972. (ADAMS Accession No. ML081140547)
16. NEDO-20953-A, *Three-Dimensional BWR Core Simulator*, General Electric, January 1977. (ADAMS Accession No. ML070730687)
17. NEDO-10527 Supplement 1, *Rod Drop Accident Analysis for Large Boiling Water Reactors: Addendum No.1 Multiple Enrichment Cores with Axial Gadolinium*, General Electric, July 1972. (ADAMS Accession No. ML081140547)
18. NEDC-33173P-A, *Applicability of GE Methods to Expanded Operating Domains*, General Electric, February 2006. (ADAMS Accession No. ML062270618)

**Enclosure 3**

**MFN 10-276**

**Affidavit**